TAMPEREEN TEKNILLINEN YLIOPISTO
TAMPERE UNIVERSITY OF TECHNOLOGY
Julkaisu 667 • Publication 667

Helmi Keskinen

Synthesis of Nanoparticles and Preparation of Deposits by Liquid Flame Spray

Tampere 2007

Tampereen teknillinen yliopisto. Julkaisu 667
Tampere University of Technology. Publication 667

Helmi Keskinen

Synthesis of Nanoparticles and Preparation of Deposits by Liquid Flame Spray

Thesis for the degree of Doctor of Technology to be presented with due permission for public examination and criticism in Sähkötalo Building, Auditorium S1, at Tampere University of Technology, on the 18th of June 2007, at 12 noon.

Tampereen teknillinen yliopisto - Tampere University of Technology
Tampere 2007

ISBN 978-952-15-1784-6 (printed)
ISBN 978-952-15-1839-3 (PDF)
ISSN 1459-2045

Abstract

There is currently immense interest in flame-generated particulate materials, and various hi-tech applications are benefiting from the great strides in development. This thesis work concentrated on the production of several single-component and composite nanoparticles and nanoparticle deposits by the flame method known as Liquid Flame Spray (LFS). In this method, the liquid precursor is atomized as micron sized droplets into a high temperature (~3000 K) hydrogen/oxygen flame, using one of reactant gases as the atomizer. The particle production rates ranged from 0.02 to 120 g/h, and the particle sizes were in the range of ~2-60 nm.

The nanoparticles and nanoparticle deposits produced in line with the work described in this thesis possess a real potential for many technological applications, such as: catalysts, self-cleaning surfaces, capacitors, and antibacterial surfaces. The scale-up of nanoparticle and deposit production from the laboratory for use in real technological applications demands a comprehensive understanding of particle synthesis in the flame. The first objective of this thesis involved gaining a thorough understanding of the particle generation process. The produced deposits were then tested for photocatalytic functionality. Photocatalytically active surfaces have been associated with desirable products like, for instance, self-cleaning windows and air/water purification systems.

Metallic silver, palladium, and silver/palladium alloy nanoparticles were successfully produced by LFS. Deposits consisted of a few nanometers silver particles were also generated. Metal salts (in water or in alcohol) were used as precursors. The water-based precursors are independent of the combustion process, while the combustion energy of the flame is increased due to the alcohol-based precursors. The inorganic precursors were almost completely evaporated in the flame. During the natural cooling along the flame, the particles nucleated and grew in accordance with typical aerosol growth processes. The resulting metallic particles were observed to be spherical. When nanoparticles were produced, the particle size was controlled by adjusting the particle production rate. The size of the silver particle deposits was also related to the deposit collection distance and time.

Nanoparticles containing iron were produced by LFS, from metal salt and water precursors, were also studied in this thesis. The particles increased in size according to the particle production rate, and consisted of pure iron, hematite, and magnetite – the majority being of geometrical morphology.

The capacity of LFS to produce ceramics such as silica and titania, using metal-organic precursors in alcohol solution, was also investigated. As with the silica particle production, also the computational fluid dynamics (CFD) was used to model the flame temperature, species vapor concentration, and saturation ratio and particle formation in the flame. The particles resulting after the flame were agglomerates. As expected, the primary and agglomerate size of the ceramic nanoparticles also increased with the particle production rate. At lower liquid feed rates, hard agglomerates were synthesized. In the titania studies, at higher particle production rates (associated with higher liquid feed rates) the soft agglomerates were generated. The titania particles consisted of anatase and rutile.

Metalorganic/inorganic/alcohol- single precursors were used to produce the titania/silver nanoparticles. Silver has a diminishing effect on the titania primary and agglomerate size; it interferes with the titania grain growth. The resulting particles were a few-nanometer sized silver particles supported by tens-of-nanometer sized titania particles.

Finally, the principal part of this study involved titania and titania/silver deposit production, by collecting the deposits both inside and just after the flame. The titania/silver deposits were made by both the one- and two-step methods. The deposits where collected on glass and steel substrates, and consisted of tens-of-nanometer sized titania agglomerates encrusted by independent few-nanometer sized silver particles. The functionality of the deposits as photocatalysts was tested by means of *Deinococcus geothermalis* biofilm 'killer' and stearic acid decomposition on surfaces under UV-illumination. While all the produced surfaces were active, the flame made one-step titania/silver deposit has the highest potentiality as photocatalyst.

In summary, single component metallic or ceramic nanoparticles, and composite metal/metal and ceramic/metal deposits were successfully produced. As well as, the silver, titania and titania/silver deposits were synthesized. The functionality of these titania and titania/silver deposits as photocatalysts was also demonstrated. However, from all of the studies in this thesis, one specific challenge concerning the nanoparticle production remains: even though the precursor evaporation was agreed to be effective, some incomplete precursor evaporation was still observed. This process leads to the formation of some larger residual particles, and especially when used at higher production rates (for technological applications) or at lower ones (for thin film applications), this will pose a problem that must be solved. Key issues to address this include perfect atomization and more easily processed precursors. In the future also the health effects during and after production of these nanoparticles or deposits must be investigated.

Preface

The studies related to this thesis were carried out in the Aerosol Physics Laboratory, Institute of Physics, Tampere University of Technology (TUT). I wish to express my gratitude to my supervisor Doc. Jyrki Mäkelä for supervising and supporting my thesis work, and also providing versatile research challenges for these studies. I also like to thank our head of the group Prof. Jorma Keskinen for his precious comments and advice during the studies.

The work was funded by the Graduate school of TUT, the Finnish Funding Agency for Technology and Innovation PINTA technology program (Tekes), Finnish Academy, Ecocat Oy, Finnish Academy of Science and Letters, and Emil Aaltonen foundation. Without these contributions these studies would not have been possible.

I especially appreciate the excellent work of my co-authors. Thanks, all of you who have been made your hands dirty while producing particles with me in lab: Tomi F., Jyrki M., Maria N., Janne L., Santtu S. and Mikko A. For the morphology analysis I'd like to thank the Institute of Material Science. Especially Dr. Minnamari Vippola and Tomi Kanerva deserved thanks for careful and enthusiastic studies with numerous nanoparticles which were observed on the TEM-grids. For the modeling study I'd like to thank all co-authors and especially Maria Nurminen, Prof. Antti Oksanen and Anna Pitkänen. The Tekes PINTA program SHINEPRO network was the best possible collaboration group to provide studies for these deposits' easy-cleaning properties. I really appreciate my co-authors work with this study. Prof Tapio Mäntylä who was leading the network gave a lot of valuable advises. Thanks also to: Mari Raulio for introducing a new friend *Deinococcus geothermalis* to me, Viljami Pore for stories about photocatalysis, and Sami Areva and Cilaine Teixteira for precious analyses.

I'd like to thank Veli-Pekka Plym for providing several 'prototypes' during the studies with this thesis. My artistic blood likes to thank the group of the glass coloring for keeping these inspiring studies going on during the years. I like to also thank the ongoing FUNCOAT network for providing new challenges with deposition production. Merit for fluent English language in my thesis belongs to Jari Schabel; thanks. Thanks are devoted for valuable and advisable comments with revision of my thesis to the thesis preliminary inspectors Dr. Lutz Mädler and Dr. Albert Nasibulin.

I had wonderful time in Prague with interesting studies- It's a beautiful town and I am grateful to Dr Pavel Moravec, Jiri Smolik and whole group from Aerosol laboratory from ICPF, Academy of Sciences of the Czech Republic. I was also very appreciative of the visit to at Prof. Sotiris Pratsinis Particle Technology Laboratory in ETH, Zürich. Thanks to this group for the pleasant and instructive visit.

I really appreciate the warm and energetic working atmosphere in the Aerosol Physics Laboratory group during the years. All of you have made our group to be one-of-a-kind. Especially, I'd like to thank Annele V., Kati V., Jyrki R., Topi R., Antti R., Ari L., Marko M., and actually whole group for the several friendly advice from measurements technique problems to very practical ones. Every composition of our substantial small 'flame-lab' has been precious

and effective. Thanks for the administrative tasks as well as many pleasant summer and Christmas seminars will belong to Inkeri Vänskä and Jaana Saaristo.

During this long journey I have been produced many salty droplets from moments of failure and success. I really appreciate my mother, sister, other relatives, and friends supporting and loving me throughout the difficult times as well as their heartfelt joining of the moments with joy and laughter. My final thanks go to the poetry:

HYMNI TULELLE

Ken tulta on, se tulta palvelkoon.
Ken maata on, se maahan maatukoon.
Mut kuka tahtoo nousta taivahille,
näin kaikuu kannelniekan virsi sille:

Mit' oomme me? Vain tuhkaa, tomua?
Ei aivan: Aatos nousee mullasta.
On kohtalosi kerran tuhkaks tulla,
mut siihen ast' on aika palaa sulla.

Mi palaa? Aine. Mikä polttaa sen?
Jumala, henki, tuli ikuinen.
On ihmis-onni olla kivihiiltä,
maan uumenissa unta pitkää piiltä,
herätä hehkuun, työhön, taisteloon,
kun Luoja kutsuu, luottaa aurinkoon,
toteuttaa vuosisatain unelmat,
joit' uinuneet on isät harmajat.

On elon aika lyhyt kullakin.
Siis palakaamme lieskoin leimuvin,
tulessa kohotkaamme korkealle!
Maa maahan jää, mut henki taivahalle.

Eino Leino (*Pyhä kevät, 1901)*

Tampere 18.5.2007
Helmi Keskinen

List of publications

The thesis consists of the following publications:

I. Mäkelä J.M., Keskinen H., Forsblom T. and Keskinen J. (2004). Generation of Metal and Metal Oxide Nanoparticles by Liquid Flame Spray Process, *Journal of Material Science* Vol.15, Issue 8, pp.2783-2788.

II. Keskinen H., Mäkelä J.M., Vippola M., Nurminen M., Liimatainen J.K., Lepistö T., and Keskinen J. (2004). Generation of Silver/Palladium Nanoparticles by Liquid Flame Spray, *Journal of Material Research* 19, Number 5, pp.1544-1550.

III. Pitkänen A., Mäkelä J. M., Nurminen M., Oksanen A., Janka K., Keskinen J., Keskinen H., Liimatainen J.K., Hellstén S. and Määttä T. (2005). Numerical study of silica particle formation in turbulent H_2/O_2 flame, *IFRF Combust. J.*, Article No. 200509.

IV. Keskinen H., Mäkelä J.M., Hellstén S., Aromaa M., Levänen E. and Mäntylä T. (2005). Generation of Titania Nanoparticles by Liquid Flame Spray for Photocatalytic Applications, EUROCVD-15, Electro-Chemical Society proceedings, Volume 2005-09, pp.491-498.

V. Keskinen H., Mäkelä J.M., Aromaa M., Ristimäki J., Kanerva T., Levänen E., Mäntylä T. and Keskinen J. Effect of silver addition on the formation and deposition of titania nanoparticles produced by Liquid Flame Spray, In press: will be published in *Journal of Nanoparticle Research* 2007.

VI. Keskinen H., Mäkelä J.M., Aromaa M., Areva S., Teixeira C.A., Rosenholm J.B., Pore V., Ritala M., Leskelä M., Raulio M., Salkinoja-Salonen M., Levänen E., Mäntylä M., and Keskinen J. (2006). Titania and titania-silver nanoparticle deposits made by Liquid Flame Spray and their functionality as photocatalyst for organic- and biofilm removal, *Catalysis Letters* 111, No. 3-4, pp.127-132.

Other work related to the thesis but not included are:

1. Moravec P., Smolík J., Levdansky V.V., and Keskinen H. (2004). CVD Synthesis of Multicomponent Nanosized Particles in an Externally Heated Tube Flow Reactor. (Eng) In: Nanostructured Materials and Their Applications. (Eds – W.W. Szymanski, P.E. Wagner, M. Itoh), 9-19, Facultas Verlags, Wien.

2. Keskinen H., Moravec P., Smolík J., Levdansky V.V., Mäkelä J.M., and Keskinen J. (2004). Preparation of ZrO_2 Fine Particles by CVD Process: Thermal Decomposition of Zirconium *Tert*-butoxide vapor, *Journal of Material Science Letters* 39, pp.4923-4929.

Author's contribution

The research reported in this thesis was carried out in the Aerosol Physics Laboratory at the Tampere University of Technology during the years 2002-2007 under the supervision of Dr Jyrki Mäkelä and Prof. Jorma Keskinen.

In Paper I, silver, palladium and iron oxide nanoparticles were generated using the Liquid Flame Spray (LFS) approach. The author performed most of the experimental work herself and co-wrote the paper with Dr Jyrki Mäkelä. In Paper II, composite silver/palladium alloy nanoparticles production by flame was studied. The author carried out most of the experimental work and wrote the paper.

In Paper III, silica nanoparticle formation by flame was studied by Computational Fluid Dynamics (CFD) based modeling and experiments. The CFD modeling was done by M.Sc. Anna Pitkänen who also wrote the paper. The author participated in the experiments and made contributions to the paper.

In Paper IV, ceramic titania nanoparticles and deposits made by flame were studied. The author carried out most of the experimental work and wrote the paper. In Paper V, flame made composite titania/silver nanoparticles and nanoparticle deposits were studied. The author carried most of out the experimental work and wrote the paper. In Paper VI, the functionality of these titania/silver deposits as a photocatalyst were studied. The author carried out most of the experimental work regarding the synthesis of the deposits, and wrote the paper. The chemical and microbiological analyses were done by the co-authors.

Nomenclature

Abbreviations

BET	Brunauer Emmet Teller
CFD	Computational Fluid Dynamics
CPC	Condensation Particle Counter
CVD	Chemical Vapor Deposition
DMA	Differential Mobility Analyzer
DNA	DeoxyriboNucleic Acid
DND	Direct Nanoparticle Deposition
EDM	Eddy Dissipation Model
EDS	Energy Dispersive Spectroscopy
ELPI	Electrical Low Pressure Impactor
FQE	Formal Quantum Efficiency
FSP	Flame Spray Pyrolysis
FTIR	Fourier Transform InfraRed
LFS	Liquid Flame Spray
MLCC	Multi-Layer Ceramic Capacitor
nHALO	Hot Aerosol Layering Operation
RNA	RiboNucleic Acid
SAED	Selected Area Electron Diffraction
SAXS	Small Angle X-ray Scattering
SGM	Spray Gun Modification
SMD	Sauter Mean Diameter
SMPS	Scanning Mobility Particle Sizer
SP	Spray Pyrolysis
TEM	Transmission Electron Microscopy
TEOS	Tetra-ethoxy ortho silicate – $Si(OC_2H_5)_4$
TEOT	Tetra-ethoxy ortho titanate – $Ti(OC_2H_5)_4$
XPS	X-ray Photoelectron Spectroscopy
XRD	X-ray Diffraction

Symbols

c	concentration of the precursor
d	diameter
d_{BET}	diameter measured by BET
D_p	particle diameter
dr	dilution ratio
d_{SMPS}	diameter measured by SMPS
d_{TEM}	diameter measured by TEM
h	Planck's constant
m	mass flow rate
N_{tot}	total number concentration
p	pressure in the mixture
p^{sat}	saturation vapor pressure
Q_A	volume rate of the gas
Q_L	volume rate of the liquid
S	saturation ratio
U_R	relative velocity of the gas
v	frequency of the radiation
W	Watt
μ_L	viscosity of the liquid
ρ_L	density of the liquid
σ_L	surface tension of the liquid

Table of Contents

Chapter 1

Introduction

Many recent important technological breakthroughs can be attributed to the ongoing developments in nanotechnology. When we discuss nanotechnology, nanomaterials and nanoparticles, we usually speak of dimensions smaller than 100 nm. Today's society demands smaller computers, mobile gadgetry, and durable materials with several unique properties. Nanotechnology has also an ecological ambition to produce as small an amount of undesirable waste as possible. (Luther, 2004)

A wide range of single component or composite nanoparticles can be produced by applying high temperature flame processes (Gutsch *et al.*, 2005). Flame processes also have a high potential for nanoparticle production scale-up (Mueller *et al.*, 2003). Titania, carbon black and fumed silica have all been produced by flame-based processes in quantities of 10^5 tons/year (Kodas and Hampden-Smith, 1999; Swihard, 2003). Today, also flame-made nanoparticles and nanoparticle deposits have been used for many technological applications – e.g. sensors (Teleki *et al.* 2006; Mädler *et al.*, 2006), catalysts (Strobel *et al.*, 2003; Teoh *et al*., 2007), functional polymers (Loher *et al*, 2006), solar cells (Tani *et al.,* 2002) spinels (Zachariah and Husarewich, 1991; Ernst *et al.*, 2007) and electronic industry components (Plyum *et al.*, 1993). There is still, however, some uncertainty over the health and environmental effects of nanoparticles; especially when they are produced in large quantities (Limbach *et al*, 2005; Luther, 2004).

In this thesis, the turbulent high temperature flame method known as Liquid Flame Spray (LFS) was used. This flame method was first utilized for glass coloring (Tikkanen *et al.*, 1997)

and it also has a high potential for industrial scale-up. The first goal of this thesis was to obtain a comprehensive understanding of the single-component metal and ceramic particle, and the composite metal/metal and ceramic/metal particle synthesis in LFS. Another goal was to produce the ceramic or metal/ceramic nanoparticle deposits and test their efficiency as photocatalysts. The understanding of the particle formation mechanism and growth in single component and composite systems were studied, for several precursors. These precursors consisted of inorganic metals salts and/or metal organic compounds dissolved in water or alcohol. The precursor concentration, liquid feed rate, chemical reactions in the liquid/ gas phase, decomposition temperatures, solvent combustion in the flame, and the produced material's thermophysical properties (melting temperature, viscosity, surface tension) have a clear effect on the particles produced. For nanoparticle deposits, the precursor and collection point (distance) played the most important roles.

The studies in this thesis have been reported in 6 publications. In Paper I, the synthesis of silver, palladium, iron, and iron oxide particles from inorganic salts were studied. These inexpensive precursors proved their capacity to produce metal nanoparticles. The iron precursor yielded pure iron and two oxide phases (hematite and magnetite), and the nanoparticles produced have a potential for various applications – such as catalysts and electronic devices (Kodas and Hampden-Smith, 1999). In this study, the produced particle size was proved to depend on the precursor vapor phase concentration in the flame. This fact also proved that the measured particles undergo gas to particle conversion in the process. An alternative particle formation route in the flame is via liquid to solid conversion. Particles produced via this route are the result of incomplete evaporation of the precursor and therefore have a larger particle size. This was observed by the appearance of large crystals in the flame-made ceria particle production by Mädler *et al.* (2002) and in the investigations by Jossen *et al.* (2005) considering flame-made

hollow, shell-like, or inhomogenous oxides. In both studies the larger particle formation depended on the decomposition properties of the precursor and the flame combustion energy. Although the LFS H_2/O_2-flame combustion energy is high, the incomplete evaporation still cannot be totally excluded in the LFS-process, especially at high metal salt concentrations. For these precursors, however, larger particle formation was deemed to be minor.

The next study concentrated on composite nanoparticles. In Paper II, silver/palladium alloy nanoparticles were studied. Silver-palladium nanoparticles have special application in the field in electronic devices (Nagashima *et al.,* 1991; Delarue *et al.,* 1995). The used precursors were metal salts in the same solution (so-called single precursors). The silver and palladium have complete miscibility (Massalski, 1986) in the alloy, which influences the particle's final alloy composition. Particle formation routes and bimodal particle size distributions were discussed in this paper in more detail than in Paper I.

In Paper III, ceramic silica nanoparticle formation in the flame from a metal organic precursor was studied using a numerical model of a LFS, as created with Fluent 6 (Fluent 2001). The model described in detail the distributions of velocity, temperature, and concentrations of the species, including precursor evaporation from the primary droplets, as well as the reaction in the gaseous phase – the results providing very important information (e.g. flame temperature profile, silica saturation ratio) for further studies. The calculations suggested that in the high temperature region silica exists in liquid form and solidifies after the hot zone of the flame. The flame characteristics obtained were in agreement with former experimental data as well as general observations of the flame. In this study, also particle sampling within the flame was introduced.

In Paper IV, ceramic titania nanoparticle production by LFS using a metal organic precursor was investigated. In this study, the anatase and rutile crystal form of titania were produced. The

produced particles have a slightly bimodal distribution. The nucleation particle mode from the gas-phase nucleation was anatase, and the residual particle mode from liquid to solid (hydrothermal combustion) conversion was rutile. The titania nanoparticles and deposits of these nanoparticles can be used in photocatalytic applications. Also in this study, the particles were sampled and analyzed inside the flame, which allowed the particle formation mechanism and growth in the flame to be experimentally investigated.

Paper V concentrated on production of the composite titania-silver particles and deposits. The addition of silver enhances the photocatalytic properties of the titania. The silver particle synthesis was also sampled and analyzed inside the flame. The location of the nucleation and growth mechanism for the single-component silver and titania particles were studied. Composite titania/silver deposits were produced by two methods: one-step and two-step. The addition of silver was observed to have a reducing effect on the growth of the titania particles. (Paper VI)

In Paper VI, the titania-silver nanoparticle's capability for photocatalytic applications was studied. The deposits were collected in the flame zone on a steel or glass surface. The titania deposits consisted of porous nanosized titania agglomerates (Dp ~100 nm) and primary particles (Dp ~10 nm). With the addition of silver, small spherical metal particles (Dp ~2 nm) were detected on the agglomerates. The photocatalytic activity was tested by stearic acid decomposition and biofilm removal using *Deinococcus geothermalis* as the model organism. The deposits have the capability for photocatalytic biofilm removal and stearic acid destruction; and the titania/silver deposits prepared by the one-step method have the highest potential.

This thesis is organized as follows: At first, in Chapter 2, the background and literature review of nanoparticles; where the high temperature flame reactors and their photocatalytic applications are discussed. Also the method of the LFS process development is briefly introduced. Chapter 3 describes the used precursors, particle production techniques, and the

produced particle characterization methods. The main results from the production of the metal, metal oxide and composite nanoparticles by LFS are discussed in Chapter 4 (Papers I, II, III, IV, and V). Also, the results of the modeling study associated with the silica particle production are briefly described. Chapter 5 concentrates on the production of the deposits by LFS (Papers V and VI) and details the usability of silver-titania as a photocatalyst (Paper VI). Chapter 6 contains an overall summary, and concludes with LFS produced single and composite particle and deposit synthesis, and their applicability as photocatalysts.

Chapter 2

Nanoparticle production

Nanomaterials and nanoparticles are introduced in this chapter, and the applications for the produced particles and the principle of photocatalysis (especially in case of titania) is also described. Aerosol processes for nanoparticle production are then also discussed, and a brief overview on the history of flame technique and especially the LFS process is given.

2.1 Nanomaterials

When a given material's dimensions are below 100 nm, it can be classified as a nanomaterial. One nanoparticle may contain several tens to hundreds of atoms or molecules. At these dimensions, nanomaterials don't anymore behave as what one would expect from the conventional macro-material. (Luther, 2004) For example, the electrical conductivity (Grass *et al.*, 2006) or melting point (Sanz *et al.*, 2002) of materials has been reported to change in the nanomaterial domain. Tailoring nanomaterials will open up a completely new material field of study (Gutsch *et al.*, 2005). The research of nanomaterials has developed rapidly in past decades – due especially to the recent developments of the nanomaterial characterization equipment, and the availability of these to researchers.

Nanosized particles can be used in many applications. Some examples of the applications already found for the particles produced in this study are described below. Nanosized silver and palladium particles have found applications in electronics, especially now that the electronic components get down to nanoscale form (Kodas and Hampden-Smith, 1999). Nanometric-scale silver, palladium, and iron particles have many catalytic applications (Kodas and Hampden-Smith, 1999) and nanosized iron oxide particles have applications in magnetic nanomaterials

(Craik, 1975; Cabanas *et al.*, 1995). Silver-palladium particles already have applications especially for electronic devices. Conductive films made from the particles produced from silver/palladium pyrolysis have been studied (Nagashima *et al.*, 1991). Multilayer ceramic capacitors (MLCC) have been fabricated using fine Ag-Pd alloy particles (Pluym *et al.*, 1995), while metal alloy particles have a high technological potential in developing conductive plastics. Silica (SiO_2) nanoparticles are widely used in applications such as toothpaste, thickening and gelling agents, and optical fibers (Kammler and Pratsinis, 1999).

Photocatalysis is the most noteworthy current application for nanosized titania and titania/silver particles/deposits. In photocatalysis, spontaneous chemical reactions near the certain material (photocatalyst) are induced by absorbed light. These chemical reactions may involve the decomposition of compounds such as organic acids, etc. and hence, photocatalysts find uses in purification technology. The chemical reactions are quick and the photocatalyst itself remains stable, while contaminants both air or water can be eliminated. One of the most studied semiconductor photocatalyst materials is titania (Fujishima, 1972). Absorbed light will result in electron excitation on the titania material surface. The surface of the titania material contains electron hole pairs and holes which can oxidize hydroxides or water, and then free electrons reduce the oxygen molecules to radicals (O_2*, OH*). The resulting radicals are strong oxidizers which can decompose organic species. The photocatalytic activity can be increased by increasing various additives. Metal ion (i.e. V, Cr, Mn, Fe, Co, and Ni) doping decreases the electron excitation energy (Paola *et al.*, 2002; Umebayashi *et al.*, 2002; Teoh *et al.* 2007). The wavelength of the light can then be increased, and from a practical point of view, the application's functionality can be transferred from the UV to the visible light spectrum. Silver doping has also been shown to increase the photocatalytic activity of titania (Abe *et al.*, 1999; Subramanian *et al.*, 2001 & 2003). For silver doping does not affect the excitation energy.

Instead, silver particle on titania will trap the photo-induced charge carriers. thereby improving the charge transfer processes and resulting in more radicals on the photocatalyst surface.

2.2 Aerosol processes for nanoparticle production

The main manufacturing processes for nanomaterial production can be classified as one of the following: 1) mechanical procedures (ball milling, etc.), 2) liquid phase reactions (sol-gel technique, etc.), and 3) gas-phase reactions (flame methods, CVD, etc.). Basically, there are two ways to generate nanoscale materials: 1) use energy (mechanical, chemical, etc.) to break bulk material into smaller pieces, or 2) build up the nanomaterial from smaller pieces at the molecular level. (Luther, 2004) Most aerosol processes for producing nanoparticles involve gas-phase reactions. Aerosol processes always involve a process step where solid or liquid particles (from molecule size to 100 μm) are in a gaseous phase (Kodas and Hampden-Smith, 1999). Usually solid, liquid, or gaseous species are decomposed by radiation energy (flame, plasma, laser, etc.) and nanoparticles are then formed by chemical reaction or condensation from the vapor phase. Aerosol processes require energy to build up the nanomaterial. Many methods based on aerosol processes (such as flames (Ernst *et al.*, 2007), furnace reactors (Nasibulin *et al*., 2007), plasma reactors (Chen *et al*., 2007) and laser ablation (Seto *et al.*, 2006) have been reported to successfully produce different composite nanoparticles (Kodas and Hampden-Smith, 1999). The material field has grown rapidly year after year and these methods are now capable of producing even very complicated multiphase nanoparticles.

2.2.1 Brief history of high temperature flame reactors

The main force behind the development of contemporary aerosol flame reactors was fumed silica (aerosil), which has had industrial importance already since the 1940s. Titania particles are the next most well studied product made by flame, and the first patent in the flame synthesis area

was related to titania and silica production (Mezey, 1966). The next noteworthy steps were taken by Ulrich (1971) who produced important scientific articles about flame synthesis. However, all the early flame reactors used gaseous precursors (halides) for particle production – i.e. injection into premixed diffusion flames. But the use of gaseous precursor was limiting the amount of compounds that were able to be produced by flame (Pratsinis, 1998). In 1971, Marshall *et al.* introduced a simple flame method for the determination of zinc oxide fumes in air. Likewise, Sokolowski *et al.* introduced in 1977 the 'in-flame reactor' method for alumina particle production. These studies were the first steps towards liquid based flame methods.

In modern spray flames, liquid precursors are now common. Atomization of the droplets was done separately before the flame or using one of the reactant gas as atomizer. The liquid feeding of the precursors has broadened the production of nanoparticle materials by flame reactors. Flame Spray Pyrolysis (FSP) has since been of interest for many researchers and entire research laboratories have been built up around this area of study. The research interest (activated also by industry) and research technology development have together further progressed spray flames to the stage where pure or mixed oxides (Mädler *et al.,* 2002; Jossen *et al.,* 2005), metals (Paper I; Grass *et al.,* 2006), doped ceramics (Johannessen *et al.*, 2002), quantum dots (Mädler *et al.,* 2003), photocatalytically active nanorods (Height *et al.*, 2006), alloys (Paper II), and even more complicated multiple compounds containing nanoparticles (Strobel *et al.,* 2006; Chang *et al.,* 2005) and functional deposits (Paper VI; Mädler *et al.*, 2006) can be produced by liquid injection based flame reactors.

2.2.2 Liquid Flame Spray process in a nutshell

In 1994, Tikkanen *et al.* published an article that dealt with glass coating by flame spraying, where glass powders were fed into a high temperature oxygen-acetylene flame. Three years later, the same group was granted a patent on a 'method and equipment for spraying material'

(Tikkanen *et al.*, 1997a) and at same time they published the scientific article on 'characteristics of the liquid flame spray process' (Tikkanen *et al.*, 1997b). This publication and patent introduced the new method known as Liquid Flame Spray (LFS). In LFS, the liquid feedstock was atomized into a high temperature turbulent H_2/O_2 flame using one as the burning gas and the other as the atomizing gas. In the next paper, glass coloring by LFS was studied (Gross *et al.,* 1999). In fact, the objective of coloring glass inspired the development of this method. At the same time, Spray Pyrolysis (SP) was in the spotlight in the field of material production by aerosol methods (Messing *et al.,* 1993; Gurav *et al.,* 1993). In SP the liquid is conventionally fed into a tubular reactor. LFS is a variation of SP where a turbulent high temperature flame is present, and it is closely related to the method known as Flame Spray Pyrolysis (FSP). FSP has today been brought to a level of controlled particle production (Kammler *et al.,* 2001; Mädler *et al.,* 2002) and high particle production rates by Mueller *et al.,* 2004. The main difference between these methods is that FSP typically makes use of a supporting CH_4/O_2 flame to ignite the dispersed (by $–O_2$) precursor that acts as a fuel itself (e.g. ethanol, toluene), resulting in a self-sustaining spray (with micron sized droplets; Heine and Pratsinis, 2005) flame. In LFS, a H_2/O_2 flame is present and the solvent part of precursor can be integrated into the fuel (e.g. ethanol) or separated from the combustion process, and may even be used to cool the flame (e.g. water). In LFS, the first particulate material production aimed studies concentrated on ceramics such as Al_2O_3, Mn_2O_3, and ZrO_2 particle production from inorganic salts and organometallic precursors (Karthikeyan *et al.,* 1997). Thereafter, the metals Ag and Pd, ferrous oxides (Paper I) and composite Ag/Pd (Paper II) nanoparticles from metal nitrate/water solutions were studied. The next study considered silica particle production from a metalorganic (tetra-ethoxy ortho silicate TEOS) alcohol (ethanol) solution (Paper III). The final three studies all involved titania particle production from a metalorganic (tetra-ethoxy ortho titanate; TEOT)

alcohol (ethanol) solution (Papers IV, V, and VI). In the last two studies, composite ceramic/metal (titania/silver) particle (Paper V) and deposit (Papers V and VI) production was investigated. In the last study, also the applicability of the material as a photocatalyst was shown (Paper VI). LFS developments have also led to the creation of the industrial and commercial applications such as direct nanoparticle deposition (DND) for optical fiber manufacture (Liekki Oy, Rajala *et al.,* 2003), and the hot aerosol layering operation (nHALO) technique for colored glass (nCOLOR) and clean surfaces (nCLEAN) applications (Beneq Oy).

Chapter 3

Methods

Several precursors were used for the nanoparticle production described in this thesis. The first section of this chapter considers the chemical and physical properties of the precursors. The relevant LFS parameters are then described, as are the produced particle sampling systems. The next sections consider the aerosol methods which were used for the size and morphology characterization. Modeling is then briefly discussed, and finally the methods for photocatalytic testing are introduced.

3.1 Precursors

The precursors for single-component particle production are listed in Table 1a, while the composite particle production precursors are introduced in Table 1b. For the silver/palladium particles production, single precursors containing both elements were used (Table 1b: G; Paper II). For the titania/silver particles (or deposits) production, both separate (from Table 1a: F, B) and single precursors (Table 1b: H) were used (Papers V and VI). Some of the physical properties of these dissolved elements and solvents at room temperature are presented in Table 2.

Table 1. a) Used precursors and the nitrate or ethoxide molarities in the precursor solutions for single-component particle production.

Precursor			***c* precursor (mol/l)**		**Papers**
			from	**to**	
A	Silver nitrate in water	$AgNO_3$ in H_2O	0.02	0.93	I
B	Silver nitrate in ethanol	$AgNO_3$ in C_2H_5OH	0.002	0.01	IV
C	Palladium tetra-amine nitrate in water	$Pd(NH_3)_4NO_3$ in H_2O	0.04	0.44	I
D	Iron(III) nitrate nonahydrate in water	$Fe(NO_3)_3 \cdot 9H_2O$ in H_2O	0.01	0.18	I
E	Silicon tetra-ethoxide (TEOS) in methanol	$Si(OCH_2CH_3)_4$ in CH_3OH	3.70	3.70	III
F	Titanium tetra-ethoxide (TEOT) in ethanol	$Ti(OCH_2CH_3)_4$ in C_2H_5OH	0.26	0.54	VI V IV

Table 1. b) The precursors, component 1 molar-%, and the nitrate and/or ethoxide molarities in the used precursor solutions for composite particle production.

Precursors				***c* precursor (mol/l)**		**Papers**
	Component 1	**Component 2**	**Molar-% of component 1**	**from**	**to**	
G	$AgNO_3$	$Pd(NH_3)_4NO_3$ in H_2O	10, 50, 90	0.10	1.00	II
H	$AgNO_3$	$Ti(OCH_2CH_3)_4$ in C_2H_5OH	~ 0.5, 1, 2, 4	0.10	0.25	IV

Table 2. The physical properties of the dissolved element and solvent at room temperature.

	T_b/$_{decomp}$ (^{o}C)	**μ (mPas)**	**σ_L i (mN/m)**
H_2O	100[1]	1.002[1]	72.8[1]
C_2H_5OH	78.5[1]	1.2[1]	22[1]
$Si(OCH_2CH_3)_4$	169[2]	0.72[1]	
$Ti(OCH_2CH_3)_4$	150-155[3]	60-80[3]	
$AgNO_3$	444[1]		
$Pd(NH_3)_4NO_3$	250[1]		
$Fe(NO_3)_3 \cdot 9H_2O$	125[1]		

[1]CRC [2]Jang, 1999 [3]Dupont, 2001

In Papers I, II, and IV, metal nitrates of Ag, Pd, and Fe were used in water solution (Table 1a: A, B, C, D). The boiling points of these silver, palladium and iron nitrates are 444, 250, and 125 (decomposition temperature only available) °C, respectively (Table 2). The melting points for

silver, palladium and iron are 961.93, 1552, and 1535 °C, and the boiling points are 2212, 3140, and 2750 °C, respectively.

In Papers III, VI, V, and IV, the metal alkoxides TEOS and TEOT were used (Table 1a: E, F). The overall reactions for thermal decomposition of these metal alkoxides are (Kodas and Hampden-Smith, 1999):

$Si(OC_2H_5)_4 \rightarrow SiO_2 + 4C_2H_4 + 2H_2O$

$Ti(OC_2H_5)_4 \rightarrow TiO_2 + 4C_2H_4 + 2H_2O$

It is also possible that oxygen from the surrounding atmosphere leads to the thermal combustion reaction of TEOS and TEOT as follows:

$Si(OC_2H_5)_4 + 12O_2 \rightarrow SiO_2 + 8CO_2 + 10H_2O$

$Ti(OC_2H_5)_4 + 12O_2 \rightarrow TiO_2 + 8CO_2 + 10H_2O$

Both of these combustion reactions produce water. Therefore, it is important to also take into account the hydrothermal combustion of TEOS and TEOT (Kodas and Hampden-Smith, 1999):

$Si(OC_2H_5)_4 + 2H_2O \rightarrow SiO_2 + 4C_2H_4 + 4H_2O$

$Ti(OC_2H_5)_4 + 2H_2O \rightarrow TiO_2 + 4C_2H_4 + 4H_2O$

It has been estimated that TEOS and TEOT thermally decompose in the presence of oxygen well below 500 °C (boiling points in Table 2) (Jang, 1999; Ha *et al.*, 1996).

3.2 Spray flame process parameters

In the LFS method, a turbulent, high-temperature H_2/O_2 flame is used. A photo of the LFS process is shown in Figure 1. The liquid precursor is atomized into micron-sized droplets (Tikkanen *et al.*, 1997) by high velocity flow and introduced into the flame where they evaporate. The evaporated compounds decompose and the reaction product re-condenses into the product species.

Figure 1. Photograph of the LFS process (SGM 2).

The liquid precursor was fed into a patented, specially designed spray gun (Tikkanen *et al.,* 1997a). Figure 2 shows illustrations of the two spray gun modifications (SGMs) used in this study: SGM 1 (used in Papers I, II, and IV), and SGM 2 (used in Papers III, V, and VI). The liquid was introduced via the center needle capillary with a cross-sectional area of 1.3×10^{-6} m^2 (SGM 1) and 3.2×10^{-7} m^2 (SGM 2). The atomizing gas was introduced through an annular ring around the center needle; the cross-sectional area of the atomizing gas ring being 2.6×10^{-6} m^2 (SGM 1) and 3.1×10^{-7} m^2 (SGM 2) (Table 3). The atomizer is in the middle of the tip of the gun and is surrounded by a ring for annular oxygen (Papers I and II) / hydrogen (Papers III, IV, V, and VI) flow, which is used as both reactant and atomizing gas. The next outer ring is for nitrogen (only used in Papers III, IV, and V) flow and the outermost ring is used for the supply of hydrogen (Papers I and II) / oxygen (Papers III, IV, V, and VI). The purpose of the nitrogen

flow between the hydrogen and oxygen is to keep the flame out of the torch head (Papers IV, III, and V). Reactants, H_2 and O_2, were supplied in a stochiometric ratio. The flows for H_2 and O_2 were 80 l/min and 40 l/min in Papers I and II, 40 l/min and 20 l/min in Paper IV, and in Papers III, V, and VI, the flows were 20 l/min and 10 l/min, respectively. The N_2 was used only in Paper III, where the flow was 10 l/min. The flow rates of the gases were controlled by a mass flow meter (Brooks, Model 0154). The calculated initial gas velocities for the SGMs at these atomization gas flow rates were 374- 1061 m/s (Table 3).

The injection of the precursor into the spray gun was performed using an infusion pump (Harward Apparatus, MA, USA) allowing the ability to adjust the liquid feed rate manually. The liquid feed rate was varied in Papers I and II from 0.5- 8 ml/min (Precursors Table 1a: A, C, D, and G) and in Paper III it was 5 ml/min (Table 1a: E), in Paper IV from 0.5- 32 ml/min (Table 1a: F), in Paper V from 0.25- 4 ml, and in Paper VI it was 2 ml/min.

The SGM 1 is a robust modification, and it was designed for higher atomization gas flows. The SGM 2 was developed with the aim to have more cost-effective flame spraying process. The SGM 2 process allows lower atomization gas flow rates and the smaller droplet sizes. The droplet size can be roughly estimated by (Lefebvre, 1989):

$$SMD = 0.585\left(\frac{\sigma_L}{\rho_L U_R^2}\right)^{0.5} + 53\left(\frac{\mu_L^2}{\sigma_L \rho_L}\right)^{0.225}\left(\frac{Q_L}{Q_A}\right)^{1.5} \qquad \text{(Eq.1)}$$

where: σ_L is the surface tension (mN/m) of liquid, ρ_L is the density (kg/m^3) of the liquid, U_R is the relative velocity (m/s) of the gas, μ_L is the dynamic viscosity (mPas) of the liquid, and Q_L/Q_A is the volume flow rate of the liquid/gas.

The liquid properties, feed rates of gas and liquid, as well as the SGM all affect to the atomized droplet size. As seen from Table 3, the SGM, atomization gas flow rate and selected

liquid, all have a significant effect on the droplet size. By contrast, the liquid feed rate has only a minor effect. The droplet size with the SGM 1 remains substantially large (Table 3). In this study, with SGM 2, 35 % smaller droplet sizes should be reached in comparison to SGM 1 (Table 3).

Table 3. Dimensions, operating conditions and calculated droplet size for SGMs.

	SGM 1	**SGM 2**
Capillary needle (m^2)	1.327E-06	3.22E-07
Atomizing gas ring (m^2)	1.784E-06	3.14E-07
Atomization gas flow rate (l/min)	40	20
Initial velocity of gas (m/s)	374	1061
Liquid feed rate (ml/min)	0.5-32	0.25-5
Sauter mean diameter size (µm) [1]	13.36-14.02	4.71-4.81
Sauter mean diameter size (µm) [2]	8.26-8.27	2.91-2.91

* calculated from (Lefebvre, 1989)
[1] for water
[2] for ethanol

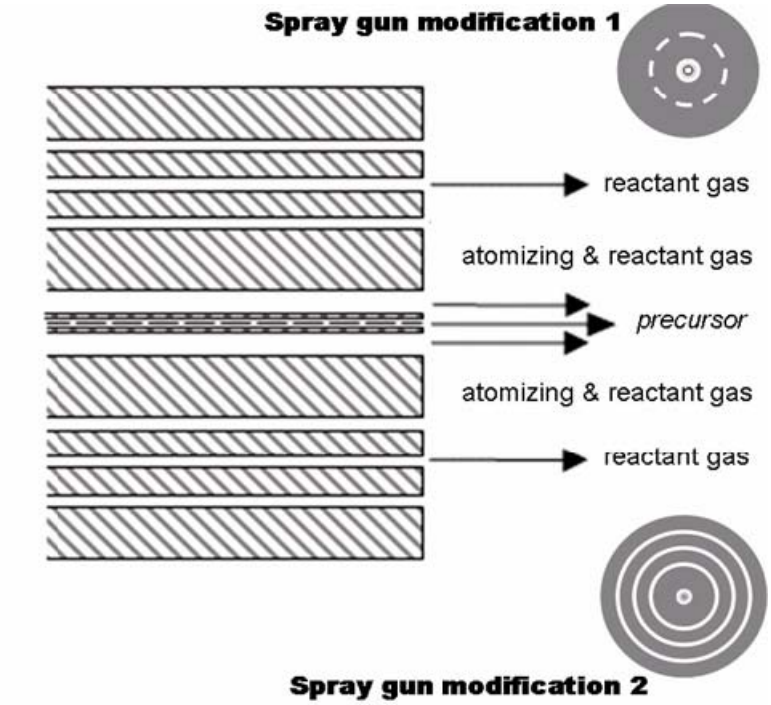

Figure 2. Illustration of the faces and cross-section of the SGMs.

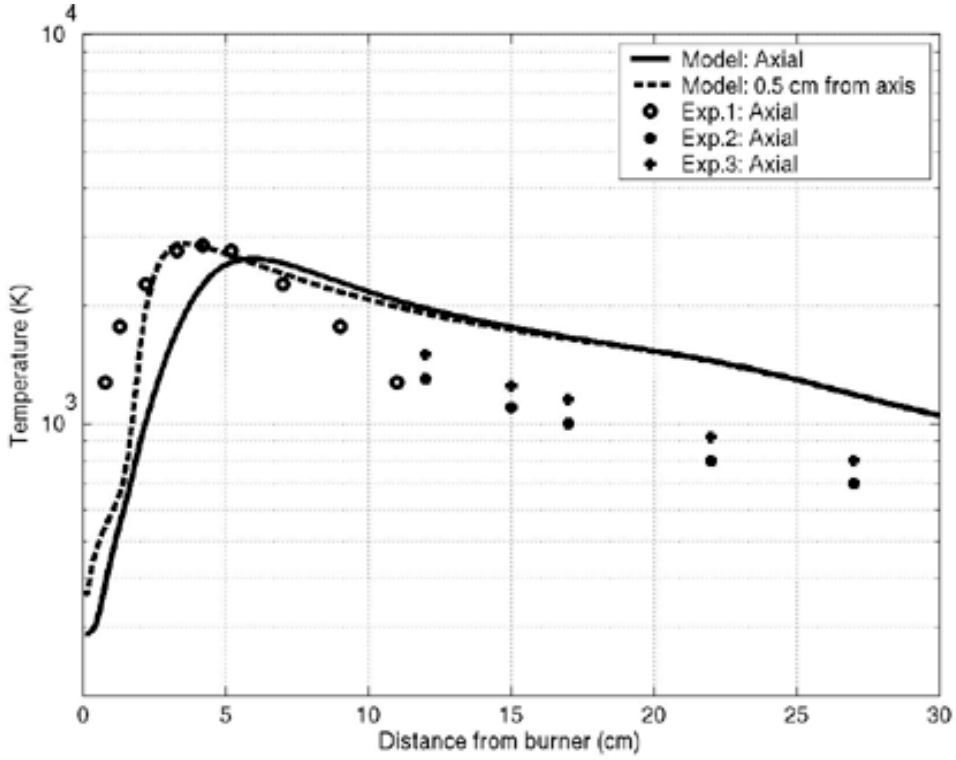

Figure 3. The axial flame temperatures for the sample collecting distances. Here, data from earlier references (Paper III (Model); Tikkanen *et al.*, 1997b (Exp1); Mäkelä *et al.,* 2006 (Exp2;Exp3)) have been combined. (Paper V)

The maximum temperature of the flame was ~3000 K and the temperature profile of the flame is shown in Figure 3 (Paper V). The solvent of the precursor and feed rate can change the flame temperature field – water can cool the flame at high feed rates and methanol/ethanol can instead elevate the temperature. The temperature field along the central axis in Figure 3 has been specified for relatively low alcohol feed rates (0- 5 ml/min). The water effect has not been measured, but it does not significantly change the visible part of flame for the feed rates (0.5-8 ml/min) used. In Paper IV, the liquid feed rate reach 32 ml/min – which clearly has an effect on the length of the visible part of the flame, and the temperature profile. At these high alcohol feed rates, the flame is longer, and so is the residence time for particle growth in the flame.

The precursor mass flow rate $m=c\cdot Q_L$ (g/min) can be controlled via the concentration c (g/l) and liquid feed rate Q_L (ml/min). In this study, the denoted mass flow rate is calculated for pure

metal compounds (Ag, Pd, Fe, Ti; Papers I, II, and IV) or produced species (SiO_2, TiO_2; Papers III, V, and VI) using their atomic weights. The mass flow rate of the precursor to the flame is also proportional to the particles' ideal production rate when the entire precursor is assumed to evaporate and convert to solid particles collected at 100 % collection efficiency. The mass flow rates used in the papers of this thesis are shown in Table 4.

Table 4. Used mass flow rates for precursors in Papers I – VI.

Precursor	Mass flow rates (g/min)		Papers
	from	to	
A	0.20	2.00	I
B	0.0004	0.0016	IV
C	0.15	0.80	I
D	0.003	0.80	I
E	1.24	1.24	III
F	0.03	1.20	VI, V, IV
G	0.01	0.80	II
H	0.002	0.04	IV

3.3 Sampling

For the aerosol measurements, the produced particle containing sample flow was diluted. The dilution system shown in Figure 4 (setup 1) was used for the LFS studies (Papers I, II, and V). In this system, the LFS gun was located at the top of the water-cooled cylindrical metal reactor (inner diameter 0.1 m), shooting the flame downwards into the reactor. The thickness of the water-cooled inner stainless steel shell of the reactor was 0.03 m and the length of the reactor was 0.6 m. The reactor had an open-end, but the walls prevented excess oxygen flow from the ambient air into the flame. The sampling probe was located 0.4 m below the flame and the exhaust gases were removed with an effective blower from the bottom of the reactor (Figure 3; setup 1). The sample flow was primarily diluted in the probe by a rotameter-controlled flow of heated compressed air and re-diluted in an ejector diluter, operating at a constant dilution ratio of 8. The total dilution ratio for the sampling system was approximately 40. (Papers I, II, and V)

Another dilution system was introduced in Paper V (Figure 4; setup 2). The most significant difference compared with the previous system is that the torch faces head-up, and the aerosol processes occur in open air (not in a reaction chamber). This open air system also has a strong dilution effect on the sample. In this system, the sample was drawn into the ejector diluter (dr ~5) (Koch *et al.,* 1988) 100 cm above the torch head using a stainless steel tube with an inner diameter of 8 mm. The total dilution ratio is impossible to define in setup 2, but it was apparently greater than the dr ~40 of setup 1. (Paper V) In both systems, the diluted sample was drawn into the aerosol measurement devices (Papers I, II, and V).

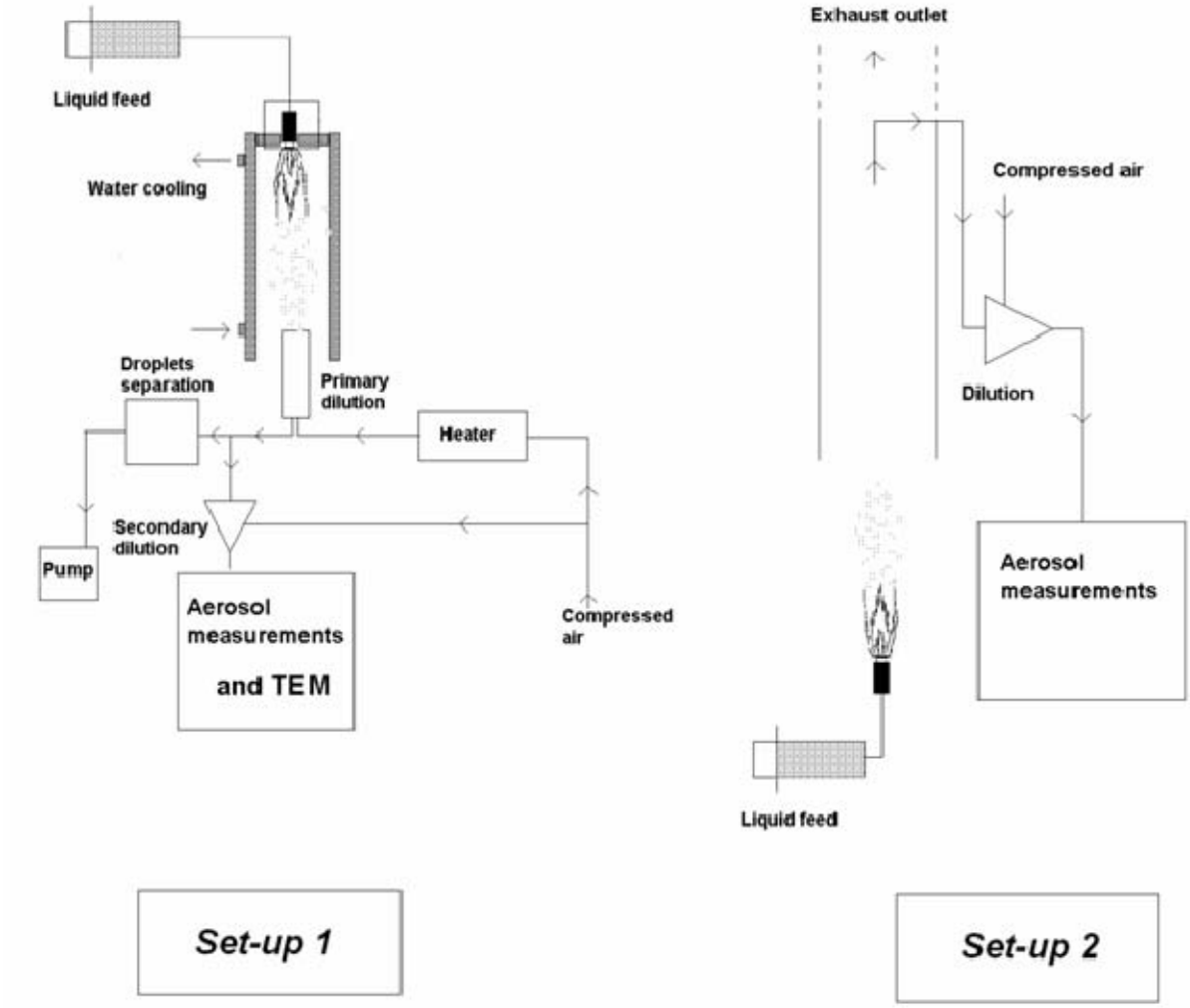

Figure 4. Schematic diagram of the LFS-process sampling setup 1 (Papers I, II, and V) and setup 2 (Paper V).

For the morphology studies by Transmission Electron Microscopy (TEM), samples of the particles were collected onto carbon coated Cu TEM grids (Agar, holey carbon/ carbon grid 300 Mesh Cu) (Papers I, II, III, IV, V, and VI). The samples were collected to TEM grids using a point-to-plate electrostatic precipitator from the sampling line for aerosol measurements, setup 1 (Papers I and II), or by direct deposition from the flame as illustrated in Figure 5: A (Papers III, IV, V, and VI). The electrostatic precipitator uses a corona discharge to charge the particles, and they are then directed by electrical forces onto a TEM grid. The sampling time for the precipitator collection was in the order of a few minutes (Papers I and II). In direct deposition from the flame, a specially designed sampling device (alumina stick with sample holder) was used (Figure 5: A). The copper grid was centered to the sample holder, and the device was then whipped through the flame – the grid being orthogonal to the flame flow. The integrated sampling time varied from approximately 2 to 10 seconds. Six collecting distances (3, 5, 10, 12, 15, and 20 cm from the burner face) for the TEM grids (Figure 4) were studied. (Papers III, IV, V, and VI).

For the silver-titania deposit production, both one- and two-step methods were studied. In the two-step method, titania particles were initially generated (Table 1a: F) and the layer of titania particles was then coated by silver particles (Table 1a: B). The two-component deposit production by the one-step method was done using a single mixed precursor (TEOT and silver nitrate in same solution; Table 1b: G). The silver additions were 1, 2, 4, and 8 –wt% (of TiO_2). In Paper V, the deposits were collected only on the TEM grids (Figure 5: A). In Paper VI, the deposits for (X-ray Photoelectron Spectroscopy) XPS-, organic- and biofilm studies were collected on the substrate from the flame at 5- 7 cm from the flame torch (Figure 5: B). The substrates were glass or steel plates and the integrated deposition time from 20- 1200 s.

In Papers V and VI, the particles were also collected in a powder form after the flame (at 50 cm from the flame torch head) using a cylindrical (diameter of 10 cm) electrostatic precipitator with a high voltage wire in the center. The collection system was similar to that described by setup 2 (Figure 4). The powder collection time was in the order of 30 min. The particles were scrubbed from the cylindrical tube and Small-angle X-ray Scattering (SAXS) and X-ray Photoelectron Spectroscopy (XPS) nitrogen adsorption to obtain specific surface area were used.

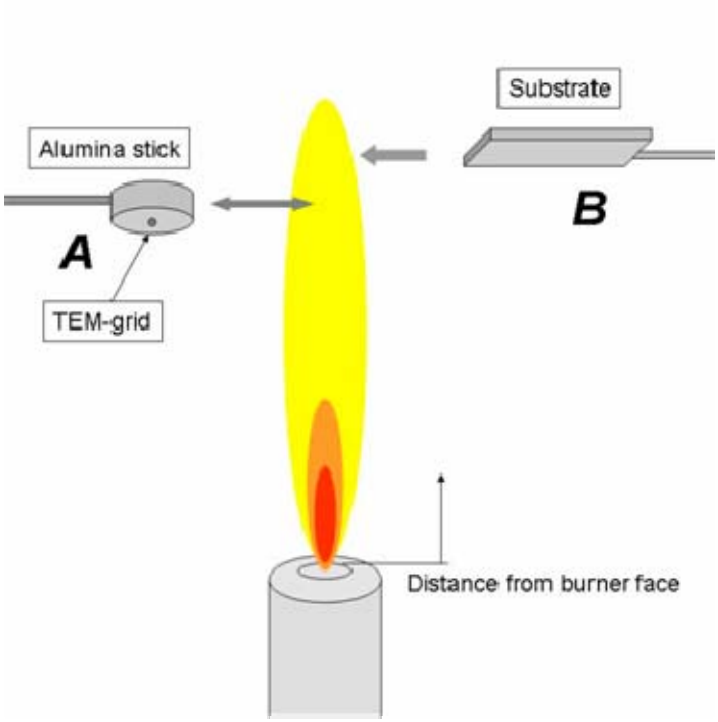

Figure 5. Illustration of the TEM sampling (Papers III, IV, V, and VI) and deposit collection from the flame (Paper VI).

3.4 Particle size characterization

For the aerosol measurements, the diluted sample was drawn into: Scanning Mobility Particle Sizer (SMPS) (Papers I, II, and V) and Electrical Low Pressure Impactor (ELPI) (Papers I, II, and V). The SMPS consists of a differential mobility analyzer (DMA) and a condensation particle counter (CPC). In the SMPS studies, the DMA (TSI model 3071A) and CPC (TSI model

3025A) were used. The SMPS (Wang and Flagan, 1990) measures the number size distribution in the range of 10- 1000 nm based on the classification of particles due to their electrical mobility in the gaseous phase, and on detection of the particles due to condensation nuclei counting. The ELPI (Keskinen *et al.*, 1992) is based on particle pre-charging and aerodynamic size classification in the particle size range of 30 nm - 10 μm, and was used with a measurement cycle of 1-5 seconds. Therefore, it was used as a real-time detector to monitor the stability of the particle number production rate during the measurements. Also, from the SMPS and ELPI data, it was possible to estimate the effective density of the particles (Virtanen *et al.*, 2004).

3.5 Morphology characterization

For the particle morphology studies, the copper grids were subsequently examined with the Transmission Electron Microscope (TEM) JEM 2010 from Jeol (Tokyo, Japan) (in Papers I, II, III, IV, V, and VI). The analyses of elemental composition were carried out by energy dispersive spectroscopy (EDS), using a Noran Vantage ThermoNoran (The Netherlands) connected to a TEM, and a Thermo-Noran D-6823 connected to a SEM (Hitachi S-4700). For the elemental mapping studies, a TEM equipped EDS was used (Jeol JEM 2010 and ThermoNoran (Paper II); Jeol JEM-100CX II and Link AN10/25S (Paper V)). The crystalline structure of the samples was investigated by selected area electron diffraction (SAED) connected to a TEM, and by X-ray diffraction (XRD) (Kristalloflex D-500, Siemens (Papers I and IV)).

The powders and deposits were analyzed by XPS (Papers V and VI). The XPS spectra were recorded using a Physical Electronics Quantum 2000 ESCA instrument. The measurements were performed at a base pressure of 1×10^{-9} torr using an Al K_α X-ray source. The pass energy for low and high resolutions spectral acquisition was 117.4 and 23.3 eV, respectively. The specific surface area was determined by gas adsorption (N_2) (Coulter Omnisorp 100 CX, Florida, USA)

using Brunauer Emmett Teller (BET) theory. (Papers V and VI) The powder samples in Paper V were studied with small-angle X-ray scattering (SAXS), with a Kratky compact camera and a Seifert ID-3003 X-ray generator operating at a maximum of 50 kV/40 mA – Cu K_α radiation was used. The system was equipped with a position-sensitive detector consisting of 1024 channels of 55.9 mm each and a sample-detector distance of 277 mm. The detector was calibrated using Silver Behenate (d-spacing = 58.38 Å), and the camera was positioned in a vacuum in order to minimize the scattering from the air. The powders were measured while in glass capillaries of an external diameter of 2 mm. Before filling the capillary with the sample, the scattering curve of the empty capillary was obtained and used as the background, which was then subtracted from the measured curve.

3.6 Modeling

In Paper III, the modeling of the synthesis of the silica particles by LFS was studied using the commercial Computational Fluid Dynamics (CFD) software Fluent 6.0. In this thesis, only the results of this study are utilized, and therefore, the modeling is only briefly introduced here.

The distributions of the three velocity components, pressure, the two turbulence quantities, temperature (enthalpy), and the mass fractions of the species in the flame were modeled by CFD. In the combustion model, the droplet input was described as "injection" and the feeding of the gases were described as "inlets into a cylindrical furnace". The diameter and length of the reactor tube are 100 and 500 mm, respectively.

Both the saturation ratio and nucleation rate are essential in the context of this thesis. The saturation ratio S is the ratio of the component pressure p in the mixture (here: SiO_2) and the saturation vapor pressure p^{sat}.

$$S = \frac{p}{p^{sat}} \qquad \text{(Eq.2)}$$

The saturation vapor pressure (p^{sat}) is the pressure required to maintain a vapor in mass equilibrium with the condensed vapor (liquid, solid) at a specified temperature. When the component pressure reaches the saturation vapor pressure, the vapor starts to condense – the saturation ratio (S) is equal to unity. In under-saturated conditions ($S < 1$) and even with low values of S in saturated conditions ($S > 1$), no nucleation occurs. The critical value of S, where significant nucleation (a nucleation rate of 1 particle/cm^3/s) starts to occur depends on the temperature and the nucleating material properties, but usually lies somewhere between 1 and 5 (Hinds, 1999; Seinfield and Pandis, 1998). In this study, we have used a pragmatic value of $S = 3$ to set a nominal threshold for S, where significant nucleation starts to occur.

The reaction rates of the combustion were modeled using the Eddy Dissipation Model (EDM), which is based on the time required for the mixing of the reacting species at the molecular level (Magnussen and Hjertager, 1976). This data was used to post-compute the nucleation rate of silica from the vapor phase and to determine the spatial particle distribution. The nucleation was calculated according to classical nucleation theory.

3.7 Photocatalytic activity testing

Stearic acid ($CH_3(CH_2)_{16}CO_2H$, Aldrich, 95 %) was used as a probe molecule to study the photocatalytic activity of the different samples in Paper VI. The durability of the flame made titania and silver-titania deposits was also tested with samples which were systematically rinsed with ethanol and wiped by lint-free cloth in an effort to remove loosely adhered particles. The stearic acid coated samples were irradiated with UV light (λ = 365 nm, intensity = 0.9 mW/cm^2) and the degradation of stearic acid was monitored by FTIR spectroscopy. The photocatalytic activity of the samples was evaluated by the degradation of a thin layer of stearic acid. This reaction is widely used in the testing of photocatalytic surfaces and has been well characterized

in the literature (Mills and Wang, 2006). Although small amounts of side-products may be generated during the degradation, the overall reaction can be written as:

$$CH_3(CH_2)_{16}CO_2H + 26O_2 \xrightarrow[h\nu \geq 3.2eV]{TiO_2} 18CO_2 + 18H_2O \quad \text{(Eq.3)}$$

In this work, the amount of degraded stearic acid was quantified from IR measurements (according to Mills *et al.,* 1997) and the initial formal quantum efficiencies (FQE) were calculated for each sample. The FQE values simply indicate how many stearic acid molecules were destroyed per one incident photon.

The model bacterium used for the photocatalytic biofilm destruction studies was *Deinococcus geothermalis* E50051 (HAMBI 2411) (Väisänen *et al.*, 1998). All samples were initially disinfected (70 % ethanol) and mounted in the wells of a polystyrene plate. The wells were filled with 3 ml of culture medium (oligotrophic medium R2, Clesceri *et al.*, 1992) and inoculated with 5 vol-% of *D. geothermalis* -strain E50051 (grown for 1 day under shaking in R2 broth). The plate was covered with a lid and incubated (+45 °C in the dark) under shaking (160 rpm) for 2 days. The plates holding samples with pre-grown biofilms, submerged in water (3 mm liquid above the biofilm), were illuminated (Sylvania 18 W Blacklight Blue) [or not illuminated (control)] at 360 nm, 0.1 mW/m^2, under shaking at +45 °C for 24 h.

The cell density of *D. geothermalis* of the biofilms was measured as described by Raulio *et al.,* 2005. The samples were also briefly flooded with a fluorochrome dye (SYTO9, Molecular Probes, Leiden, Netherlands) that has an affinity for bacteria and emits a specific fluorescence only when bound to cellular DNA or RNA. The emitted fluorescence per cm^2 of test coupon was quantified using a scanning fluorometer (Nikon Eclipse E800, Tokyo, Japan). The fluorochrome emission was calibrated with preparations containing known numbers of *D. geothermalis* cells.

Chapter 4

Production of nanoparticles by LFS

In this thesis, various kinds of nanoparticles have been produced by LFS. Silver, palladium, iron oxides, silica, titania, silver/palladium, and titania/silver particles production by LFS and the produced particulate material characteristics are discussed in this chapter. The first section introduces liquid-to-solid and gas-to-particle conversions. The other results focus on the growth and characteristics of the nanoparticles formed via the gas-to particle conversion. In the last section, the modeling and experimental results are briefly compared.

4.1 Two routes

In principle, there are two possible routes for solid particle production from liquid droplets using the LFS process (Figure 6). The first route involves liquid-to-solid conversion (Mode 2; Figure 6), and the second a gas-to-particle conversion (Mode 3; Figure 6). Another pathway, a "combination-route", involves partial precursor evaporation from the droplet; where the evaporated part will progress along the second route and the residual part will continue along the first route. For the liquid-to-solid conversion, the nature of the residual particles was notably related to the precursor itself, the droplet size, and the liquid precursor concentration. The process to produce the solid particle via the first route can occur either within the flame, or already in liquid phase (hydrothermal combustion). Before the gas-to-particle conversion, the entire precursor droplet needs to evaporate. For evaporation, the most influential parameters are the droplet size, the precursor itself, the residence time of the droplet in the flame, and the flame temperature profile. The evaporation should be more effective for ethanol and SGM 2 because the droplet size remains smaller (Table 3). After evaporation in the gas-to-particle conversion,

the final particle size and morphology was most significantly affected by the precursor itself and the precursor concentration in the flame.

When nitrate water solutions were used as a precursors (Papers I and II), both modes were detected. In the first two studies (Papers I and II), the particle size analysis was based on the number size distributions which were measured by SMPS/ELPI. For silver, palladium, silver/palladium, and iron oxide particles, the nucleate mode clearly dominated the number size distributions. The same size was also obtained at different precursor concentrations c (changing the liquid feed rate Q_L such that the mass flow rate $m=c\cdot Q_L$ remained constant). Both these observations indicated that the particles were mainly synthesized by gas-to-particle conversion (Figure 6; Papers I and II). Still, some residual particles were observed from the TEM-images, and these residual particles are most probably formed by the first route (due to incomplete evaporation of the largest droplets). In Paper IV, a low concentration ethanol/silver nitrate solution was used as the precursor, resulting in substantially low mass flow rates. Therefore, the flame was capable of vaporizing the precursor, and very few nanometric scale (Paper V) residual mode particles were detected using TEM imaging.

In the LFS process, some water vapor always exists; it is a combustion product from H_2/O_2 flame. Water is also a by-product of the thermal decomposition or hydrothermal combustion of the metal alkoxides. It should also be noted that methanol and ethanol have an affinity to water, and therefore, hydrolysis is already possible in the precursor solution stage, even before the liquid is sprayed into the flame. When metal organic precursors (Papers III, V, IV, and VI) in alcohol solution were used, the hydrothermal combustion (introduced in Chapter 3.1) played a crucial role in the formation of residual particles. For silica particle production (from TEOS/methanol) only few residual particles were detected (Paper III). Somewhat more (but still not many) were detected in the titania (from TEOT/ethanol) studies (Papers V, IV, and VI). The

silica or titania particles formed already in the liquid stage will most probably not evaporate in the flame. Instead, they will simply condense and form crystals. Those particles which hydrolyze already in the liquid stage, and those particles which are formed by liquid-to-solid conversion, both act as a condensation sink for the vapour and therefore they decrease the precursor mass from the nucleate mode (Mode 3; Figure 6). In all the studies, the nucleate mode (Mode 3; Figure 6) formed via the second route clearly dominated the measured number size distributions of the particles.

4.2 Particle growth in gas-to-particle conversion

When considering gas-to-particle conversions, the measured number concentration and number size distributions provide relevant information. Figure 7a shows the total number concentration (N_{tot}) of the particles as a function of time during the iron oxide particle synthesis experiment (measured by ELPI). This measurement was done at a constant liquid feed rate 2 ml/min while increasing the precursor concentration. The corresponding mass flow rates were: 1) 0.005, 2) 0.01, 3) 0.015 g/min. As one can see from Figure 7a, the number concentration rises very quickly after the flame has been ignited. Just after ignition, the N_{tot} was not usually stable – probably due to two reasons: A) air bubbles entering during the liquid feed, and B) liquid feed rate temporarily increasing during ignition. After stabilization, the N_{tot} remained quite constant – even as the mass flow rate was increased during the experiment. In Figure 7b, the number mean size distributions for these three mass flow rates are shown. In all studies, an increase in the mass flow rate (particle production rate) (Papers I, II, IV, and V) was associated with an increase in the mean particle size (primary or/and agglomerate) (example from iron oxide production Figure 7b). The size was measured by SMPS/ ELPI or/and TEM. For example, for the same mass flow rate 0.01 g/min the mean particle size (measured by SMPS) was ~17 nm for Fe_xO_y (Figure 7b, (2)),

~14 nm for the Ag/Pd-alloy particle, and ~20 nm for the composite TiO_2/Ag particle (Papers II and V).

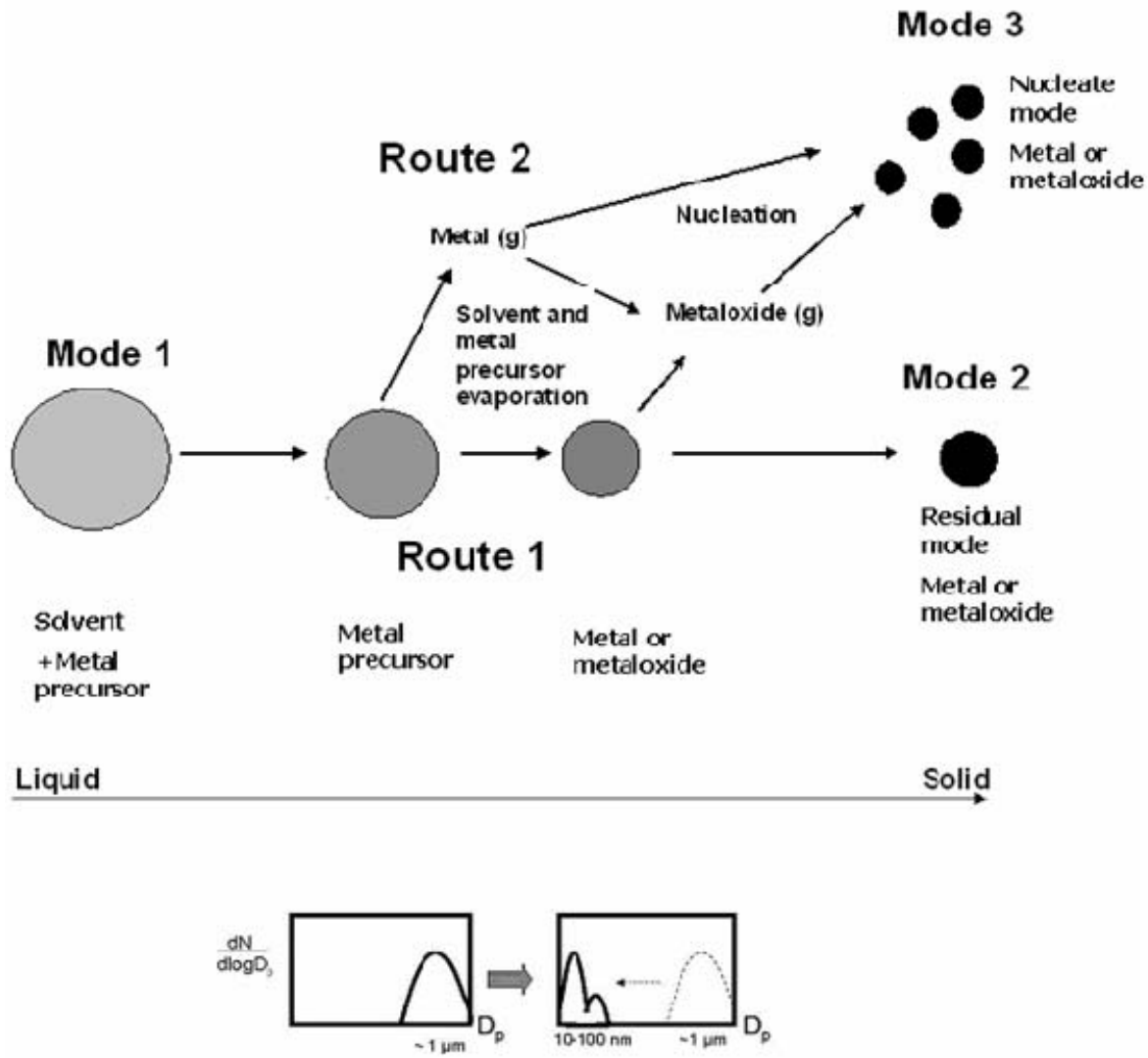

Figure 6. Overview of particle formation from liquid-to-solid by the LFS process.
Mode 1: Primary spray droplets; Mode 2: Spray pyrolyzed residual particles (created by *Route 1*); and Mode 3: Nucleated nanoparticles from gas-to-particle conversion (created by *Route 2*, major route in this work). (modified from: Kodas and Hampden-Smith, 1999; Paper II).

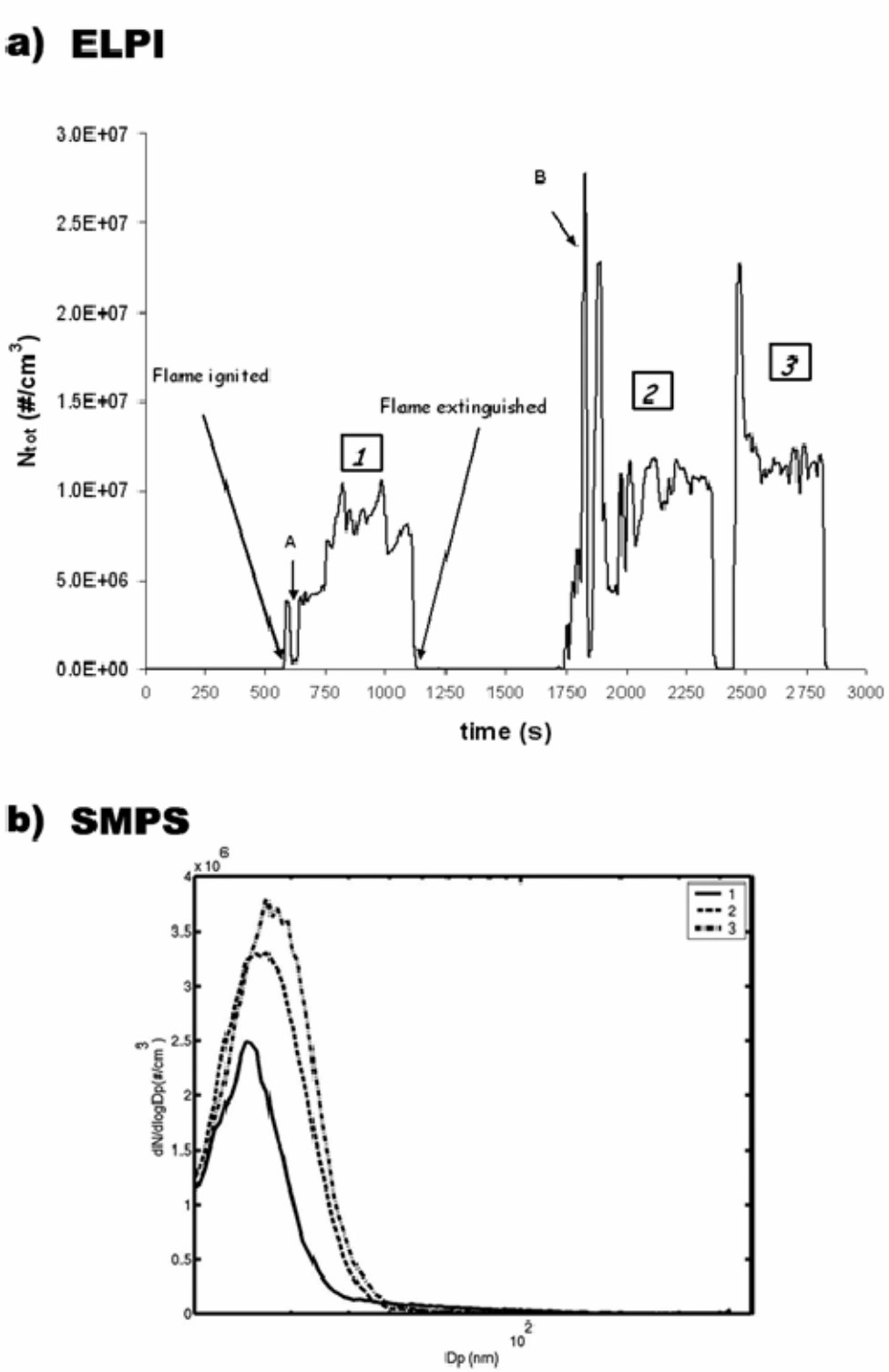

Figure 7. a) Iron oxide particles number concentration as a function of time (by ELPI), and b) size distributions measured by SMPS at mass flow rates 0.005 (1), 0.01 (2), and 0.015 g/min (3).

The regions in the flame where the saturation ratio (*S*) will be greater than 1, can be determined using the evaporated component of metal or metal oxide concentration in the flame (e.g. mass

flow rate) and assuming a certain flame temperature profile (Figure 3, Table 5). Nucleation is expected to start at this point (Chapter 3.7 and Table 5), and after this point, the particles will grow by surface growth, coagulation, collisions, sintering/coalescence and agglomeration. The particle growth in the flame always involves collisions and coalescence. If the final shape of the particle is a solid sphere, the dominant growth mechanism will be collision limited; while if the end shape is an agglomerate, coalescence will limit the growth (Lehtinen *et al.,* 1996). The initial particle growth in the flame is always collision limited. The produced particulate material and the mass flow rate will mainly determine whether the growth becomes coalescence limited during the flame process (Lehtinen *et al.,* 1996). In Table 5, a simplified indicative magnitude to coalescence and collision times is presented for the particle synthesis in the flame, when the mass flow rate and produced particulate material changes (Note: liquid feed rate effect omitted).

Table 5. Simplified table of mass flow rate and product influence to saturation ratio, coalescence and collision times in particle synthesis by LFS in this thesis.

	Mass flow rate		**Metal**	**Ceramic**
	low	**High**		
S > 1 in the flame	later	earlier	later	earlier
Coalescence Time [1]	same	same	shorter	longer
Collision Time [1]	longer	shorter	same	same

[1] particle size is assumed to be constant

Two kinds of agglomerates can be generated by the flame process: soft and hard (Tsantilis and Pratsinis, 2004). The soft agglomerates are independent particles which are connected to each other only by weak van der Waals forces, while the hard ones are sintered to each other and connected by much stronger forces. The growth will change from collision to coalescence limited at a certain point in the flame. The location of this point, together with the particulate material sintering properties, determines the particle shape after the flame.

The morphology of the particles produced in this thesis is described in Figure 8. In Papers I, II, and V, the studied silver, palladium, iron oxides, and silver/palladium particles (at the certain

mass flow rates; Figure 8: 1, 2, 3, 4, 8) all had a collision limited growth mechanism. Only soft agglomerates were detected after the flame – most probably formed during the collection stage when directed by electrical forces. There is a possibility that at higher mass flow rates the agglomeration can occur earlier, however, no TEM samples were taken at these higher mass flow rates (Papers I and II; Table 5).

In Paper III, the silica particle production at one mass flow rate was studied. In the case of silica, the growth was initially collision limited but changed to coalescence limited within the flame. Hard silica agglomerates were then produced (Figure 8: 5). The particles collided with each other and coalesced/sintered somewhat, but remained as agglomerates with a visible neck formation. For titania (Papers IV and V), a wider mass flow rate range was studied. The hard titania agglomerates were produced at a lower mass flow rate (Figure 8: 6). Higher mass flow rates (Paper IV) instead produced soft agglomerates (Figure 8: 7). At the higher mass flow rate, a greater number of primary particles were present. Due to the higher liquid feed rate the flame was also longer – indicating a longer residence time. The primary particles therefore have more time to coalescence and achieve a spherical morphology in the flame. (Papers V and IV)

For composite one-step titania/silver particles, the morphology analysis was done at one mass flow rate (0.04 g/min). The produced particles were hard agglomerates (Figure 8: 9) and the growth was coalescence limited. From the measured particle size distributions the predicted number mean particle size (d_{SMPS}) was very small ~10 nm at the lowest (0.002 g/min) mass flow rate (Paper V). The mass flow rate may have been sufficiently low to ensure that the particle growth remained collision limited. The addition of silver to the precursor decreased the particles' primary and agglomerate size, in comparison with the pure titania particles. The decrease in the particle size is most likely due to the depression effect of silver on the titania (anatase) grain growth (Paper V).

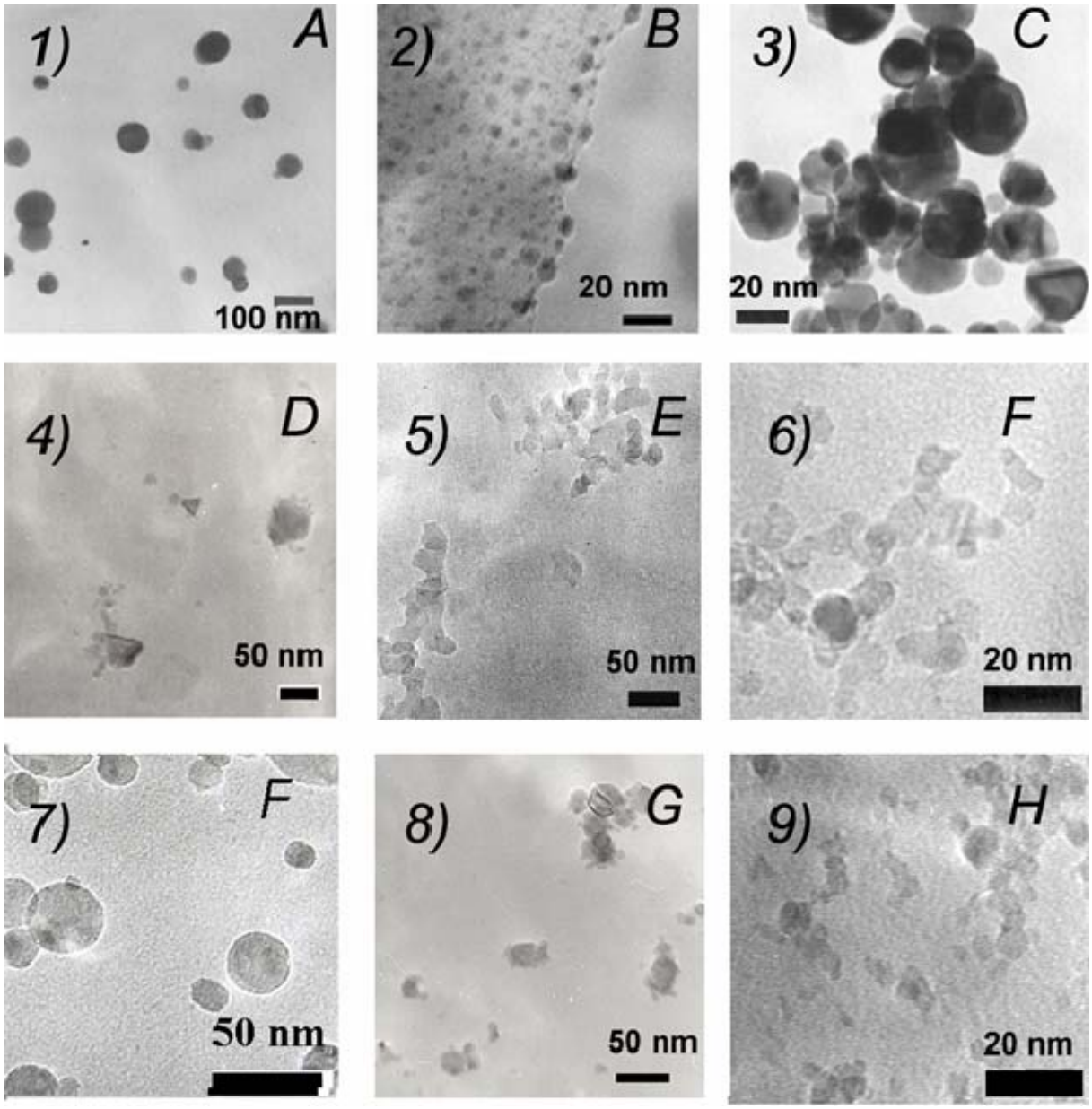

Figure 8. TEM micrographs from LFS produced particles: 1) Ag at m = 2.5 g/min (A); 2) Ag at 0.0016 g/min (B); 3) Pd at 0.26 g/min (C); 4) Fe_xO_y at 0.26 g/min (D); 5) SiO_2 at 1.24 g/min (E); 6) TiO_2 at 0.04 g/min (F); 7) TiO_2 at 1.2 g/min (F); 8) Ag/Pd/ (50/50 molar-%) at 0.2 g/min (G); and 9) TiO_2/Ag at 0.04 g/min (H). (Letters A-H are connected to the used precursors; Tables 1a & 1b)

4.3 Composition

The shapes of the particles produced during this thesis work are shown in Figure 8. Also, the composition of the particles was studied. In Paper I, the composition of the particles was verified

by XRD at certain mass flow rates. The metal particles were pure silver and palladium. The iron oxide XRD-spectrum consisted of pure Fe, hematite (α-Fe_2O_3), and magnetite (γ-Fe_3O_4). The composite silver/palladium composition was analyzed by EDS and elemental mapping. The particles were deemed to be alloys and the molar ratio of metals in the precursor determined the final particle alloy composition (silver/palladium ratio in the particle) (Paper II).

In Paper III, the particles were assumed to be SiO_2, but the composition was not experimentally verified. In Papers IV and V, the titania particle composition was verified by SAED at a certain mass flow rate, and the small agglomerates (Figure 8: F) comprised of anatase crystal structure. Instead, the residual mode particles (assumed formed by hydrothermal combustion) had a rutile crystal structure.

The verification of the composite titania/silver particle (one-step, single precursor) morphology and composition was quite challenging (Papers V and VI). It was impossible to determine individual titania and silver particles directly from the TEM micrograph (Figure 8: H). The elemental mapping predicted that the silver was uniformly distributed on titania agglomerates and residual particles consisted only of titania (Paper V). The SAXS and XPS studies concluded that silver was present as independent spherical particles (of a few nm in size) on the titania agglomerates (Paper V). These analyses, however, do not exclude the possibility that the silver particles were partly contained within the titania agglomerate. Nevertheless, no bond between the titanium and silver, or the silver and oxygen, was detected. The titania/silver deposits were also studied (Chapter 6).

Simultaneous measurement by both SMPS and ELPI gives an approximate value for the density of the particles (Virtanen *et al.*, 2004). The effective density was studied for LFS made silver (Paper I) and titania/silver (Paper V) particles. An effective density of 10.58 g/cm^3 for silver particles was obtained (Ristimäki *et al.*, 2002). The bulk density of silver is close to the

measured value 10.5 g/cm. This indicated that the silver particles consist of pure metal and are relatively spherical in shape.

The effective density studies were also carried out for titania/silver for a mass flow rate 5.8 mg/min with silver addition 1- 4 % (setup 1; Figure 4), and 0.8- 14 mg/min with silver addition 1- 8 % (setup 2; Figure 4). Due to the agglomeration of the particles, the density values were lower in comparison to the bulk density. Also, the agglomerate size measured by setup 2 (Figure 4) was close to the lower size limit of the ELPI, which made the density calculation less accurate. The method is also susceptible to particle bounce in the impactor (Rao and Whitby, 1978), which would result in decreased density values. The first observed trend was a slight increase in effective density for increased silver addition (Paper V); confirming the observation for setup 1. The density increase may be explained by the addition of higher bulk density material to the titania agglomerates. The mass flow rate also systematically influences the effective density: higher mass flows produce lower density values. With silver addition of 1 wt-% at a mass flow rate of 0.8 mg/min the effective density was 1.7 g/cm^3, and for a mass flow rate 14 mg/min it was ~1.1 g/cm^3. The same trend was observed for higher proportion silver additions, and is the result of a higher agglomeration rate at higher mass flow rates. Figure 8: H shows that the measured particles were hard agglomerates.

4.4 Comparison of modeling and experimental results

In Paper III, silica particle synthesis by LFS flame was studied. The commercial CFD software Fluent 6.0 was utilized to model the flame characteristics; including the velocities, turbulence, temperature profile, and concentration distributions. In addition to the in-built models of the commercial CFD code, a new sub-model was designed to describe the nucleation of SiO_2 from the vapor phase to the liquid/solid one, i.e. particles. As presented in Chapter 3.7, classical nucleation theory was used as the fundamental item of this model. The motivation behind the

Paper III study was to obtain information about silica particles – especially concerning their formation in flames – by creating a simple but reliable model of the nucleation rate to describe the on-set of the particle formation.

Figure 3 shows the modeling results of the temperature along the central axis, while Figure 9 shows the modeled 2-dimensional temperature field of the flame. The temperature is deemed to be at it's maximum at about 2- 5 cm into the flame torch. While the LFS is always operated in open-air conditions in the work of this thesis, the modeling was instead done in an enclosed space. This may lead to a slight increase in the modeled flame temperatures. Figure 10 shows the spatial distribution of the saturation ratio in the range of $3 < S < 10$. Along the central axis, particle formation should begin after the hottest part of flame (5 cm); when also the saturation ratio is achieved ($S = 3$). At the edges of the flame, where the temperature is lower, the nucleation occurs already near the flame beginning. The TEM samples showed that particles were clearly formed already at 3 cm. (Paper III)

This study has afforded valuable information concerning the flame temperature profile. Also the modeling of the saturation ratio and the nucleation zone has been confirmed by the experimental studies and simplified calculations. The deposit synthesis will be discussed in the next chapter. These modeling studies have provided good grounds for deposit preparation by LFS.

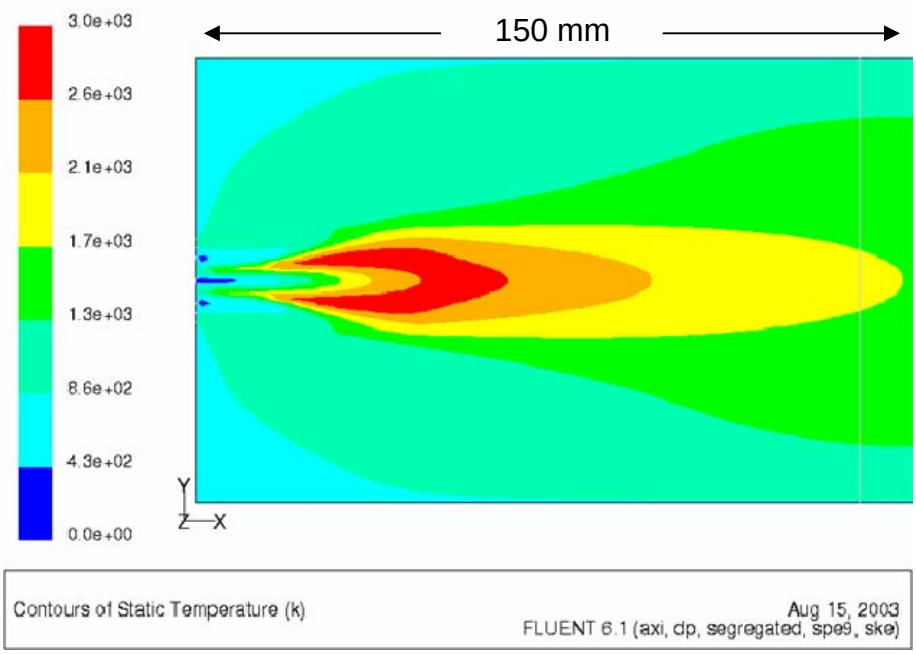

Figure 9. Two-dimensional temperature distribution of the flame up to 150 mm from the flame torch inlets. (Paper III)

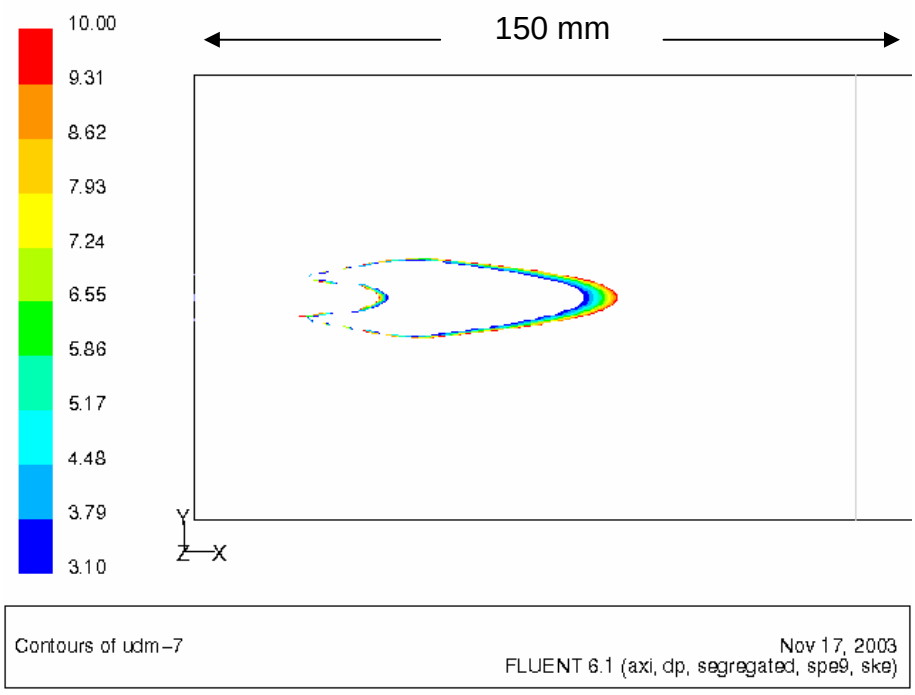

Figure 10. Spatial distribution of saturation ratio in range of $3 < S < 10$. (Paper III)

Chapter 5

Preparation of deposits and testing of their functionality as photocatalysts

Silver, titania, and titania/silver deposits were produced by LFS in this thesis work, and this chapter concentrates on the investigation of these deposits. The deposits were collected in and immediately upon leaving the flame (Papers VI, V, and VI). Also, the deposits' functionality as photocatalysts will be discussed.

For deposition collection, the collection distance and the deposition time both play important roles. The temperature at the collection distance also has a significant effect on the properties of the collected deposit (Figure 3). The precursors' evaporated metal or metal oxide component – specifically its thermophysical properties and concentration – in association with the temperature profile of the flame, determine the nucleation zone within the flame. Prior to this point, the precursor is in a gaseous form. Therefore, deposit collection before this nucleation zone involves direct gas-phase deposition. After this zone, the particles have been already nucleated in the gaseous phase before the deposition. Because the flame is turbulent and the temperature profile three-dimensional, the exact point of nucleation is quite hard to determine; even by using CFD modeling (Paper III). A simplistic way to predict the point of nucleation involves only considering the central axis temperature profile and calculating the point at which the saturation ratio (S) of the selected precursor with a certain concentration in the flame exceeds 1 (Chapter 4; Table 5). Experimental studies can then be compared to these calculations.

In Papers VI, V, and VI, silver, titania, and titania/silver deposits were studied. Composite titania/silver deposits were produced by the one- and two-step methods. Figure 11 presents the silver, titania, and titania/silver deposits collected on the TEM grid at three axial distances (5, 12,

20 cm) from the flame torch. The corresponding collection temperatures for these distances were ~3000, 2000 and 1600 K (Figure 3 (Model) and Figure 9).

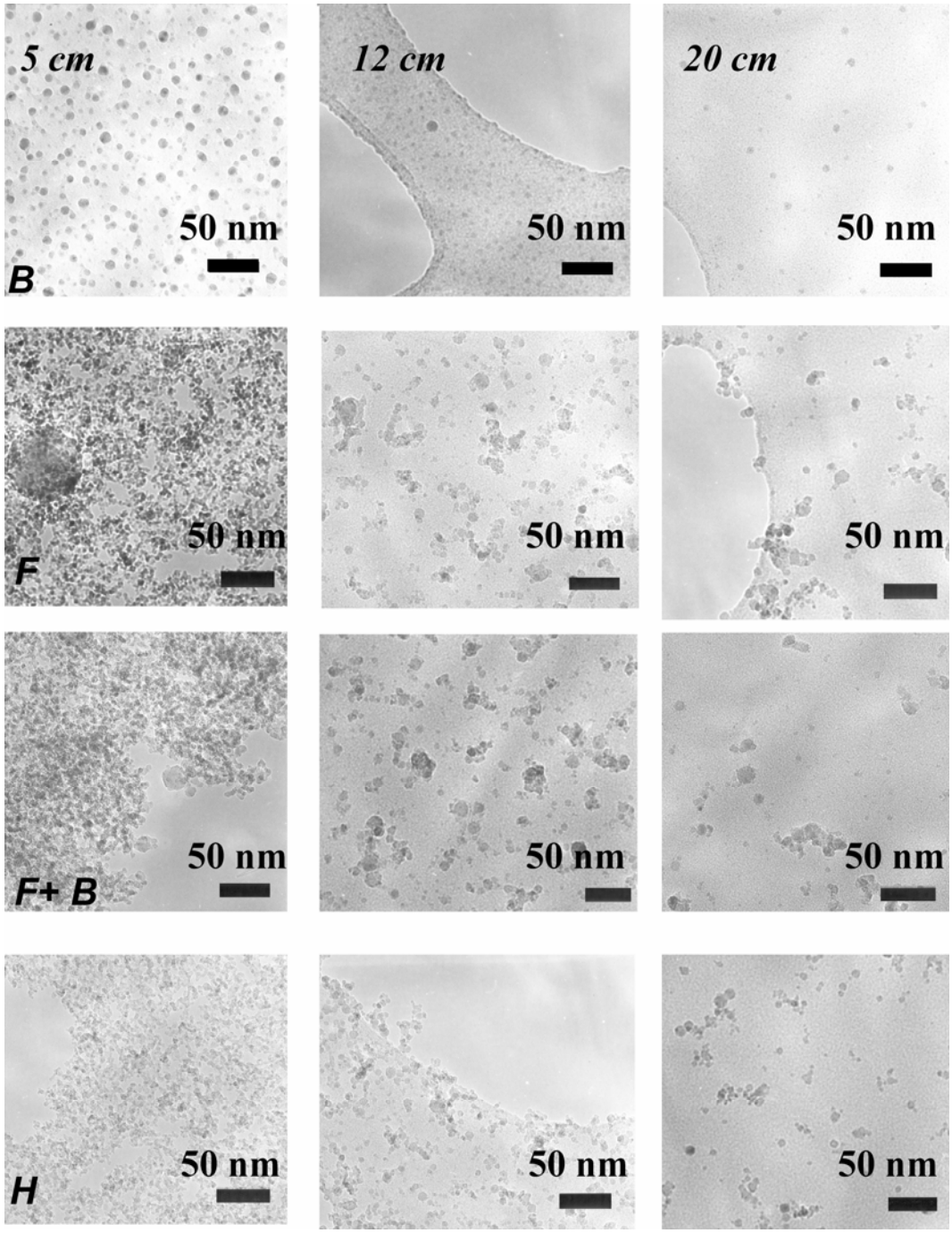

Figure 11. Ag (B) at 0.0016 g/min, TiO_2 (F) at 0.04 g/min, two-step TiO_2/Ag (F+B) at 0.04 + 0.0004 g/min, and one-step TiO_2/Ag (H) at 0.04 g/min particle deposits – at three distances (5, 12, and 20 cm) from the torch. (Sampling time ~10 s) (Letters B, F, and H are connected to the used precursors; Tables 1a & 1b)

In Paper V, two mass flow rates of the silver 0.0004 and 0.0016 g/min were studied (Table 1a: B). The nucleation point for silver in the flame for these mass flow rates was estimated by calculating the saturation ratio. For the lower mass flow rate, the location was deemed to be 14 cm from the torch head, and for the higher one, it was a marginally earlier at 12.5 cm. At distances prior to the nucleation distance, the particles on the grid were formed by direct gas-phase deposition, and the particle size was similar at both mass flow rates (Paper V). After nucleation, the particle size increased in accordance with conventional aerosol growth processes, i.e. surface growth, coagulation, and sintering. Within these studied mass flow rates the particle size remains smaller at further distances (nucleation before the deposition) compared to the closer distances (direct gas-phase deposition) (Figure 11: (B)). The growth was clearly collision limited; as was discussed in Chapter 4. (Paper V)

For titania deposit synthesis, the mass flow rate was higher (0.04 g/min). Titania was estimated to evaporate from this metal organic precursor immediately after it was introduced to the flame. Nucleation was therefore assumed to occur at least after the hottest point in the flame (~5 cm; Figure 3). As seen from Figure 11: F, at 5 cm it is impossible to predict the primary size of titania particles. Instead, at 10 cm the primary size of the hard titania agglomerates is clearly below 10 nm. In case of the titania, it is assumed that the particles have already been nucleated in the gaseous phase before deposition at any of the studied distances. When the flame ends, the titania particles reached a final primary particle size of 10 nm. The growth was collision limited; as was discussed in Chapter 4. (Paper V)

From the TEM micrograph of the composite titania/silver deposits made by the two-step method, it was difficult to see separate silver particles at closer collection distances (3, 5, 10 cm) from the flame torch (Figure 11: F+B). At these closer distances the silver could have been uniformly distributed on the titania particles layer, or enriched in certain places. At further

distances (15 and 20 cm), the primary size of the two-step deposit reached the same size as pure titania deposits (10 nm). For composite titania/silver deposits made by the one-step method, the primary particle sizes detected from the TEM micrograph were smaller (at all distances) than in deposits made by the two-step method. The silver most probably interfered with the titania grain growth; as was discussed in Chapter 4. For the one-step composite deposit, the separate titania and silver particles were directly discernible from the TEM micrographs. The elemental mapping was also carried out for the silver addition amount of 4 %, i.e. the silver particles were observed with the actual production rate of 0.0016 g/min The X-ray elemental mapping of titanium and silver for the silver addition of 4 % is shown in Figure 12a. The maps permit the observation of titania agglomerates and silver distribution in the sample. Finally, XPS and SAXS predicted that there were separate silver particles on the titania agglomerates in both the one- and two-step deposits (Figure 12b) (Paper V).

As introduced in Chapter 3.7, the photocatalytic activity of the deposits were defined by the initial FQE values. The FQE values were quite high for the titania, and composite two-step and one-step titania/silver deposits from which the loosely adhered deposits had not been removed. The samples were also tested after the loosely adhered particles had been removed. Especially the deposits of titania and one-step titania/silver had noticeable activity even after the removal of the loose particles, indicating that some active particles still remained on the surface. There were, however, fewer active sites after the removal of those loose particles. The sample produced using the one-step method seems to have the highest photocatalytic activity before removal of the loose particles. After the loose particles were removed, the titania deposit had the highest activity. (Paper VI)

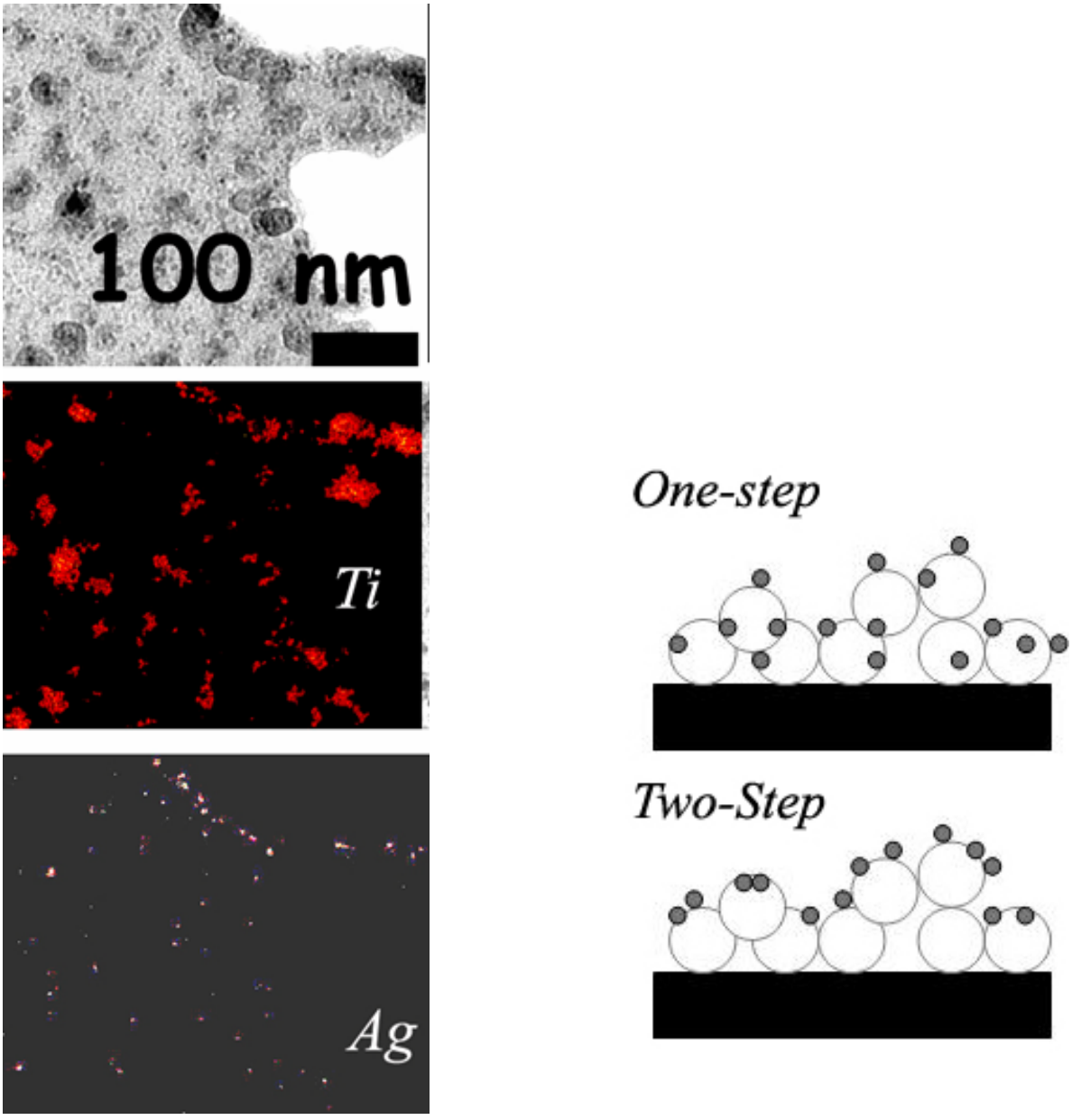

a) *b)*

Figure 12. a) X-ray elemental mapping for a sample of 40 mg/min TiO_2 with 4 % silver addition (1.6 mg/min) sampled at distance of 12 cm; b) The different morphologies of two component deposits.

The tendency of the three deposits (titania, and one- and two-step titania/silver) to attract biofilm bacteria (Chapter 3.7) was compared to that of the non-coated steel substratum. In the absence of illumination, less biofilm was attracted by the coated surfaces than the non-coated

steel. The one- and two-step titania-silver deposits attracted only 3- 11×10^6 cells/cm^2 of bacteria as compared to the plain steel which had 26×10^6 adhered cells/cm^2. After illumination, only 0.2-2×10^6 cells/cm^2 remained on the coated composite samples. Illumination of the titania (H) and one-step titania-silver (I) deposits removed 97 % and 94 % of the biofilm bacteria respectively, compared to their non-illuminated counterparts. The one-step deposit was deemed to be the most efficient as biofilm growth inhibitor in the dark. (Paper VI)

It is obvious that in deposits made by the one-step process, the addition of silver increased the photocatalytic stearic acid- and biofilm removal efficiency. The reason for the lower activity of the two-step deposits was most probably due to the silver aggregation on the topmost layer of the samples (Figure 12b). This segregation layer may prevent the penetration of the illumination to the porous titania layer, and therefore the photocatalytic activity is decreased. The one-step deposits also have greater photocatalytic activity before removal of the loose material, compared with the plain titania deposits. Silver should increase the photocatalytic activity (He *et al.*, 2002). In this study, also the decreased particle size (Paper V) of the one-step samples was seen to contribute towards the increased photocatalytic activity – in line with the increasing specific surface area of the deposits. In the photocatalytic activity test, the increased activity of one-step titania/silver over titania was so slight that it may be induced by increased surface area. In the bacteria tests, the increased activity was more obvious (Paper VI) and the addition of silver should itself have elevated the photocatalytic activity of the deposit.

Chapter 6

Summary and conclusions

The first objective of this thesis involved gaining a thorough understanding of the particle synthesis in LFS. The study encompassed single component metal and ceramic particle, and composite metal/metal and ceramic/metal particle synthesis in LFS. Valuable knowledge about particle synthesis by LFS was obtained by successful use of this method in production of silver, palladium, iron oxide, silica, titania, silver/palladium alloy, and composite titania/silver nanoparticles, and by experimental investigations of the produced particles. Moreover, the second goal involved the production and testing of the nanoparticle deposits. Silver, titania and composite titania/silver deposits were produced, and the capacity of these deposits as photocatalysts was also tested.

The key parameters for particle production by LFS were related to the spray gun modification (SGM), the gas flow rates, the precursor(s), the liquid feed rate, and the mass flow rate (particle production rate). The SGM, atomization gas flow rate, precursor and liquid feed rate all define the droplet size. The mass flow rate and flame length will have main impact to the produced particle size (Figure 13).

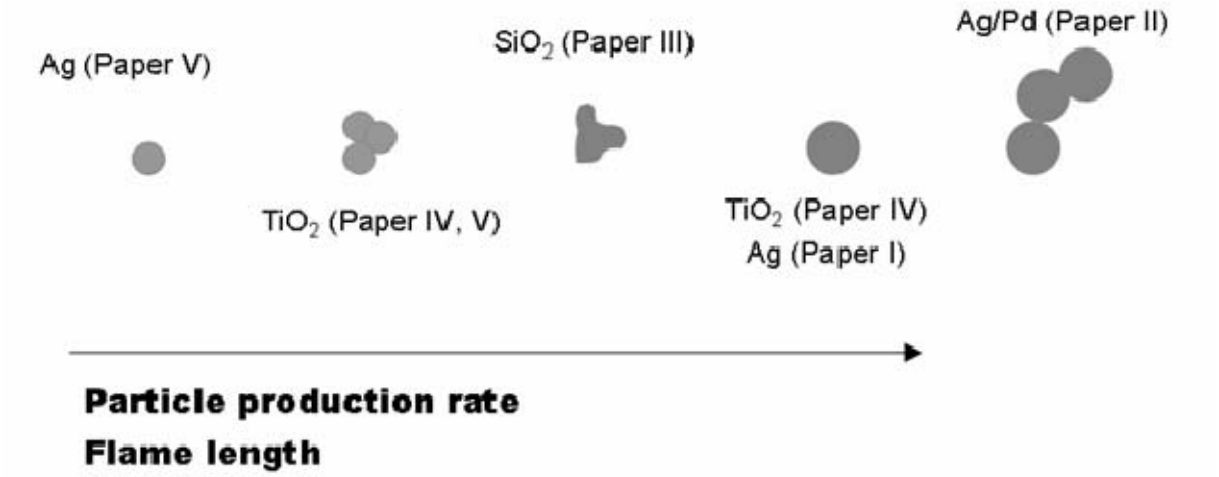

Figure 13. Illustration of particle size and morphology, as related to the particle production rate and increasing flame length, for the different particulate material produced.

Table 6 provides a summary, for precursors A-H (Table 1a; Table 1b), of single-component and composite particle properties made by LFS for a certain mass flow rate. The primary particle size has been estimated from the TEM micrographs, and the agglomerate or sphere size from the SMPS measurements. Both soft and hard agglomerates were observed – the harder ones were formed in the flame (Table 6; Figure 11: TiO_2, SiO_2) and the softer ones during the collection phase (Table 6; Figure 11: Ag/Pd). The size of the silver, palladium, ferrous oxides and silver/palladium alloy particles was collision-limited, while for silica or titania it was deemed to be coalescence-limited. From the particle size measurements and TEM micrographs, it was also observed that the primary particle (d_{TEM}) and agglomerate size (d_{SMPS}) decreases with increasing silver addition. Therefore, the silver addition decreases the primary and agglomerate particle size by interfere the particle formation; most probably during the surface growth and sintering state. Certain nanoparticles are needed for certain applications. This table can be used as a base reference to create recipes for particle production – e.g. the required particle size or morphology.

Table 6. Summary of particle synthesis and characteristics for different precursors (A-F) in LFS at certain production rates.

Precursor	**A**	**B**	**C**	**D**	**E**	**F**	**G**	**H**	**B+F**
Spray gun modification (SGM)	SGM 1	SGM 1	SGM 1	SGM 1	SGM 2	SGM 2	SGM 1	SGM 2	SGM 2
Atomization gas flow rate (l/min)	40	40	40	40	20	20	40	20	20
Molar-% of component	100	100	100	100	100	100	50	0.5	0.5
Method	one-step	one-step	one-step	one-step	one-step	one-step	one-step	one-step	two-step
Production rate (g/min)	2.50	0.0016	0.26	0.26	0.06	0.04	0.20	0.04	0.04
Size (d_{SMPS})	~55 nm	no data	~25 nm	~35 nm	no data	~80 nm [1]	~27 nm	~60 nm [1]	no data
Size ($d_{TEM/primary}$)	~55 nm	~7 nm	~25 nm	~10-25 nm	~20 nm	~10 nm	~10-30 nm	~5-8 nm	~10 nm
Shape	S	S	S	G	AGG	AGG	AGG	AGG	AGG
If agglomerates	soft	soft	soft	soft	clearly hard	hard	soft	hard	hard
Product composition	Ag	Ag	Pd *	Fe, Fe_2O_3, Fe_3O_4 *	SiO_2	TiO_2	alloy: S	TiO_2: AGG / Ag: S	TiO_2: AGG / Ag: S
Analysis method	XRD	EDS	XRD	XRD	EDS	XRD	EDS, mapping	SAXS, XPS	SAXS, XPS
Growth limited by	Col	Col	Col	Col	Coa	Coa	Col	Coa	Col (Ag) / Coa (TiO_2)
Residuals	few	very few	few	few	few	few	few	few	few

S = spheres; AGG = agglomerates; G = geometric shapes
Col = collision; Coa = coalescence
[1] at production rate 0.01 g/min.
* sample taken at higher production rate

According to the TEM micrographs, few residual particles were detected in all the studies (Table 6). In titania particle production, also a specific surface area was specified. Residuals were not affected by the particle size ($d_{TEM(primary)}$ = 10 nm, d_{BET} = 10 nm). In subsequent studies, more precise measurement techniques, besides TEM imaging about residual particles, will be needed. Considering the mass distribution, even a few residual particles can easily play a significant role. The existence of the residual particles must be noted, especially when high quality monodisperse nanoparticles are required. With regard to the avoidance of the formation of residual particles during LFS, the choice of precursor and generation of monodisperse small droplets, are key factors.

The collection of particles as a deposit directly from the flame has opened up new application areas: such as thin films for photocatalysts and solar cells. In this study, the formation mechanism for the titania and titania/silver deposits was direct gas-phase deposition onto the substrate immediately at the end of the flame torch. The mechanism changed to the conventional aerosol process (gas-phase nucleation) further away from the flame, while in between, there is a transfer zone where both mechanisms are involved in the deposit formation. The exact locations of these zones are dependent on the precursor concentration in the flame, the temperature of the deposit, the thermophysical properties of the precursors' evaporated metal or metal oxide component. The deposit morphologies are different in the one-step and the two-step methods. In the one-step method, titania particles are coated uniformly by silver particles, while in the two-step method the silver particles are only on the topmost layer of the titania particle deposit.

Photocatalytically active deposits have the potential to decompose organic dirt (Fujishima and Honda, 1972). These deposits can be used, for example, on common everyday surfaces (e.g. Pilkington Activ glass). The photocatalytic activity of the titania and composite

titania/silver deposits produced by LFS was reasonably high. Titania and one-step titania/silver deposits were also active before and after cleaning of the surface. The deposits also proved to have a capacity for photocatalytic biofilm removal and stearic acid destruction. Of all the deposits studied, the titania/silver deposits prepared by the one-step method have the greatest potential as a photocatalysts. The tests were performed on a laboratory scale with relatively small samples. Future studies should focus on the increased production of the deposits, the use of these in the real environment, and also on ready-made products (e.g. a tiled wall in the bathroom). Also the photocatalytic functionality should be investigated, taking into account the analysis of the deposit thickness and amount on the substrate. One challenge would be to shift the photocatalytic activity from UV-light to the visible light spectrum.

Liquid precursors provide us with the tool to select any soluble element from the periodic table, and atomize it to the flame to produce nanoparticles or deposits. The production of several materials by liquid based flame methods has been studied. The study field for different nanoparticle and deposit production is, however, still very wide. And especially health effects during the production should be carefully studied in the near future. Key aspects for the development of risk free production include: open inventive minds and interdisciplinary co-operation between different research groups and companies.

References

Abe, T., E. Suzuki, K. Nagoshi, K. Miyashita and M. Kaneko (1999). Electron Source in Photoinduced Hydrogen Production on Pt-supported TiO_2 Particles, *J. Phys. Chem.* B, 103: 1119–1123.

Beneq Oy, http://www.beneq.fi/ [visited 21/03/2007]

Cabanas, M.V., J.M. Gonzalez-Calbet and M. Vallet-Regi (1995). *Ceramics: Charting the Future.* p. 1221.

Chang, H., I. Lengorro, T. Ogi and K. Okuyama (2005). Direct Synthesis of Barium Magnesium Aluminate Blue Phosphor Particles via a Flame Route, *Mat. Lett.* 59: 1183-1187.

Chen J.H., G.H. Lu, L.Y. Zhu and R.C. Flagan (2007) A Simple and Versatile Mini-Arc Plasma Source for Nanocrystal Synthesis, *J. Nanoparticle Res*. 9(2): 203-213.

CRC Handbook of Chemistry and Physics 60th edn., (1979), CRC Press, Boca Raton.

Craik, D.J. (1975). *Magnetic oxides.* John-Wiley & Sons, New York.

Clesceri, L.S., A.E. Greenberg and A.D. Eaton (Eds) (1992). Heterotrophic plate count. In: Standard Methods for the examination of water and wastewater, American Public Health Association, American Water Works Association and Water Environment Federation, 20th Edition, American Public Health Association, Washington DC, USA: 9-34 to 9-36.

Delarue, E., M. Mostafavi, M.O. Delcourt and D. Regnault (1995) Characterization of silver-palladium submicronic powders, *J. Mater. Sci.* 30:628.

DuPont Tyzor (2001). http://www.dupont.com/tyzor/ [visited 13/03/2007]

Ehrman, S.H. and S.K. Friedlander (1999). Bimodal distributions of two component metal oxide aerosols, *Aerosol Sci. Technol*., 30: 259.

Ernst F.O., H.K. Kammler, A. Roessler, S.E. Pratsinis, W.J. Stark, J. Ufheil and P. Novák (2007), Electrochemically active flame-made nanosized spinels: $LiMn_2O_4$, $Li_4Ti_5O_{12}$ and $LiFe_5O_8$, *Materials Chemistry and Physics*, 101, Issues 2-3: 372-378.

Fluent 6, (2001). http://www.fluent.com/ [visited 21/03/2007].

Fujishima, A. and K. Honda (1972). Electrochemical Photolysis of Water at a Semiconductor Electrode, *Nature* 238: 37.

Grass, R.N. and W.J. Stark (2006). Flame spray synthesis under a non-oxidizing atmosphere: Preparation of metallic bismuth nanoparticles and nanocrystalline bulk bismuth metal, *J. Nanoparticle Res*., on-line web, http://www.springer.com/ [visited 21/03/2007].

Gross, K.A., J. Tikkanen, J. Keskinen, V. Pitkänen, M. Eerola, R. Siikamäki and M. Rajala (1999). Liquid Flame Spraying for Glass Coloring, *J. Thermal Spray Technol.* 8: 583-589.

Gurav, A., T.T. Kodas, T. Pluym and Y. Xiong (1993). Aerosol Processing of Materials, *Aerosol Science and Technology* 19: 4-11.

Gutsch, A, H. Mühlenweg and M. Krämer (2005). Tailor-made Nanoparticles via Gas-Phase Synthesis, *SMALL*, 1: 30-46.

Ha, H.K., M. Yoshimoto, H. Koinuma, B.K. Moon and H. Ishiwara (1996). Open air plasma chemical vapor deposition of highly dielectric amorphous TiO_2 films, *Appl. Phys. Lett.* 68: 2965.

He, C., Y. Yu, X. Hu and A. Larbot (2003). Effect of silver doping on the phase transformation and grain growth of sol-gel titania powder, *J. Eur. Ceram. Soc.* 23: 1457.

Height, M.J., S.E. Pratsinis, M. Mekasuwandumrong and P. Praserthdam (2006). Ag-ZnO Catalysts for UV-photodegradation of Methylene Blue. *Appl. Catal. B -Env.* 63: 305-312.

Heine, M.C., and S.E. Pratsinis (2005). Droplet and Particle Dynamics during Flame Spray Synthesis of Nanoparticles, *Ind. Eng. Chem. Res*., 44 (16): 6222-6232.

Hinds, W.C. (1999). *Aerosol Technology*, John Wiley & Sons, New York, p.284.

Jang, H.D. (1999). Generation of Silica from Tetraethylorthosilicate (TEOS) Vapor in a Diffusion Flame, *Aerosol Science and Technology* 30: 477-488.

Johannessen, T. and S. Koutsopoulos (2002). One step Synthesis of an Active Pt/TiO_2 Catalyst for SO_2 Oxidation – A Possible Alternative to Traditional Methods for Parallel Screening. *J. Catal.* 205: 404-408.

Jossen, R., S.E. Pratsinis, W.J. Stark and L. Mädler (2005). Criteria for flame-spray synthesis of hollow, shell-like, or inhomogeneous oxides, *J. Am. Ceram. Soc.* 88: 1388.

Jossen, R., R. Mueller, S.E. Pratsinis, M. Watson and M.K. Akhtar (2005). Morphology and Composition of Spray-flame-made Yttria-stabilized Zirconia Nanoparticles. *Nanotechnology.* 16: 609-617.

Kammler, H.K., L. Mädler and S.E. Pratsinis (2001). Flame synthesis of nanoparticles, *Chem. Eng. Technol.* 24: .583-596.

Kammler, H.K. and S.E. Pratsinis (1999). Scaling-up the production of nanosized SiO_2-particles in a double diffusion flame aerosol reactor, *J. Nanoparticle Res.,* 4: 467-477.

Karthikeyan, J., C.C. Berndt, J. Tikkanen, S. Reddy, J.Y. Wang, A.H. King and H. Herman (1997). Preparation of nanophase materials by thermal spray processing of liquid precursors. *Nanostructured materials* 9: 137-140.

Keskinen, J., K. Pietarinen and M. Lehtimäki (1982). Electrical Low Pressure Impactor. *J. Aerosol Sci.* 23: 353-360.

Koch, M., H. Lödding, M. Mölter and F. Munzinger (1988). Verdünngssystem für die messung hochkonzentrierter aerosol mit optischen partikelzählern, *Staub-Reinhaltung der Luft* 48: 341.

Kodas, T.T. and M.J. Hampden-Smith (1999). *Aerosol processing of materials*, Vol. 10 and 12 Wiley-VCH, New York.

Lehtinen, K. (1997). Theoretical studies on aerosol agglomeration processes. Ph.D. Thesis, VTT/Helsinki University of Technology.

Lefebvre, A.H. (1989). *Atomization and Sprays*. Taylor & Francis, London, p.87, 233.

Liekki Oy, http://www.liekki.com/ [visited 21/03/2007].

Limbach, L.K., Y. Li, R.N. Grass, T.J. Brunner, M.A. Hintermann, M. Muller, D. Gunther and W.J. Stark (2005). Oxide Nanoparticle Uptake in Human Lung Fibroblasts: Effect of Particle Size, Agglomeration and Diffusion at Low Concentration, *Env. Sci. Technol.* 39(23): 9370-76.

Loher, S., T. Maienfisch, S. Bokorny, W. Grimm and W.J. Stark (2006). Rapid production of micropatterned surfaces using a fluid dynamical instability, *Polymer Eng. & Sci* 46: 1541-1547.

Luther, W. (2004). *Industrial application of nanomaterials – changes and risks*. Technology analysis, ISSN-1436-5928, Dusseldorf, Germany.

Mädler L., W. Stark and S.E. Pratsinis (2002). Flame-made Ceria Nanoparticles, *J. Mater. Res.*, 17**:** 1356.

Mädler, L., W. J. Stark and S.E. Pratsinis (2002). Rapid Synthesis of Stable ZnO Quantum Dots, *J. Appl. Phys.* 92: 6537-6540.

Mädler, L., A. Roessler, S.E. Pratsinis, T. Sahm, A. Gurlo, N. Barsan and U. Weimar (2006). Direct Formation of Highly Porous Gas-sensing Films by *in situ* Thermophoretic Deposition of Flame-made Pt/SnO_2 Nanoparticles. *Sens. Actuat. B-Chem.* B114: 283-295.

Magnussen, B.F. and B.H. Hjertager (1976). On mathematical models of turbulent combustion with special emphasis on soot formation and combustion, *16th Symposium (Int'l.) on Combustion.* The Combustion Institute.

Mäkelä, J.M., S. Hellstén, J. Silvonen, M. Vippola, E. Levänen and T. Mäntylä (2006). Collection of liquid flame spray TiO_2 nanoparticles on stainless steel surface, *Mater. Lett.* 60: 530.

Marshall, B.S., I. Telford and R. Wood (1971). A Field Method for the Determination of Zinc Oxide Fume in Air. *Analyst*, 96: 569-578.

Massalski, T.B., *Binary Alloy Phase Diagrams* (1986). American Society for Metals, New York, pp.54-55.

Messing, G.L., S.C. Zhang and G.V. Jayanthi (1993). *Journal of the American Ceramic Society,* 16: 2101.

Mezey, E.J. (1966). Pigments and reinforcing agents, in Vapor Deposition. (Eds – C.F. Palmer, J.H. Oxley and J.M. Blocher Jr.) Wiley, New York, pp.423-451.

Mills, A. and S. Le Hunte (1997). An overview of semiconductor photocatalysis, *J. Photochem. Photobiol. A: Chem.* 108: 1.

Mills, A., J. Wang and M. McGrady (2006). Method of Rapid Assessment of Photocatalytic Activities of Self-Cleaning Films, *J. Phys. Chem. B.*, 110: 18324-18331.

Mueller, R., L. Mädler and S.E. Pratsinis (2003). Nanoparticle synthesis at high production rates by flame spray pyrolysis, *Chem. Eng. Sci.* 58: 1969.

Nagashima, K., T. Himeda and A. Kato (1991). Properties of conductive films made from fine spherical silver-palladium alloy particles, *J. Mater Sci.* 26: 2477.

Nasibulin, A.G., P.V. Pikhitsa, H. Jiang, D.P. Brown, A.V. Krasheninnikov, A.S. Anisimov, P. Queipo, A. Moisala, D. Gonzalez, G. Lientschnig, A. Hassanien, S.D. Shandakov, G. Lolli, D.E. Resasco, M. Choi, D. Tománek and E.I. Kauppinen (2007). A novel hybrid carbon material, *Nature Nanotechnology*, 2: 156-161.

Paola, D., E. García-López, S. Ikeda, G. Marci, B. Ohtani and L. Palmisano (2002). Photocatalytic degradation of organic compounds in aqueous systems by transition metal doped polycrystalline TiO_2, *Catal. Today 75:* 87.

Pilkington, http://www.pilkington.fi/ [visited 21/03/2007].

Pluym, C.T, T.T. Kodas, L.-M. Wang and H.D. Glicksman (1995). Silver-palladium alloy particle production by spray pyrolysis, *J. Mater. Res.* 7: 1661.

Pratsinis, S.E. (1998). Flame Aerosol Synthesis of Ceramic Powders, *Prog. Energy Combust. Sci.* 24: 197-219.

Rajala, M., K. Janka and P. Kykkänen (2003). An Industrial Method for Nanoparticle Synthesis with a Wide Range of Compositions, *Reviews on Advanced Materials Science* 5: 493-497.

Rao, A.K. and K.T. Whitby (1978). Non-ideal collection characteristics of inertial impactors-II. *Journal of Aerosol Science* 9: 87-100.

Raulio, M., V. Pore, S. Areva, M. Ritala, M. Leskelä, M. Lindén, J.B. Rosenholm, K. Lounatmaa and M. Salkinoja-Salonen (2006). *J. Ind. Microbiol. Biot.* 33: 261.

Ristimäki, J., A. Virtanen, M. Marjamäki, A. Rostedt and J. Keskinen (2002). On-line measurement of size distribution and effective density of submicron aerosol particles, *J. Aerosol Sci*. 33: 1541.

Seinfield, J.H. and S.N. Pandis (1998). *Atmospheric Chemistry and Physics*. John Wiley & Sons, pp. 788-794.

Seto, T., K. Koga, F. Takano, H. Akinaga, T.I. Orii, M. Hirasawa and M. Murayama (2006). Synthesis of magnetic CoPt/SiO_2 nano-composite by pulsed laser ablation, *J. Photochem. and Photobio. A: Chemistry,* 182: 342.

Sanz, N., A. Boudet and A. Ibanez (2002). Melting Behavior of Organic Nanocrystals Grown in Sol–gel Matrices, *J. Nanoparticle Res.* 4: 1-2.

Sokolowski, M., A. Sokolowska, A. Michalski and B. Gokieli (1977). The "in-flame-reaction" method for Al_2O_3 aerosol formation, *Journal of Aerosol Science* 8: 219.

Strobel, R., W.J. Stark, L. Mädler, S.E. Pratsinis and A. Baiker (2003). Flame-made platinum/alumina: structural properties and catalytic behaviour in enantioselective hydrogenation, *J. Catal.*, 213: 296.

Strobel, R., L. Mädler, M. Piacentini, M. Maciejewski, A. Baiker and S.E. Pratsinis (2006). Two-nozzle flame synthesis of Pt/Ba/Al_2O_3 for NO_x storage. *Chem. Mater.* 18(10): 2532-2537.

Subramanian, V., E.E. Wolf and P.V. Kamat (2001). *J. Phys. Chem. B* 105: 11439-11446.

Subramanian, V., E.E. Wolf and P.V. Kamat (2003). *J. Phys. Chem. B* 107: 479-7485.

Swihart, M.T. (2003). Vapor-phase synthesis of nanoparticles. *Current Opinion in Colloid and Interface Science*, 8: 127-133.

Tani, T., L. Mädler and S.E. Pratsinis (2002). Synthesis of zinc oxide/silica composite nanoparticles by flame spray pyrolysis, *J. Mater. Sci.* 37: 4627-4632.

Teleki, A., S.E. Pratsinis, K. Kalyanasundaram and P.I. Gouma (2006). Sensing of organic vapors by flame-made TiO_2 nanoparticles,, *Sens. Actuators, B, Chem,* 119: 683-690.

Teoh, W.Y., R. Amal, L. Mädler and S.E. Pratsinis (2007). Flame sprayed visible light - active Fe- TiO_2 for photomineralization of oxalic acid, *Catal. Today,* 120: 203-213.

Tikkanen, J., M. Eerola and M. Rajala (1994). Coating glass by flame spraying, *Journal of Non-crystalline solids* 178: 220-226.

Tikkanen, J., M. Eerola, V. Pitkänen and M. Rajala (1997a). Method and equipment for spraying material. *Patent no. 98832*-Finland. (in Finnish)

Tikkanen, J., K.A. Gross, C.C. Berndt, V. Pitkänen, J. Keskinen, S. Raghu, M. Rajala and J. Karthikeyan (1997b). Characteristics of the liquid flame spray process, *Surf. Coatings Technol.* 90: 210.

Tsantilis, S. and S.E. Pratsinis (2004). Soft- and Hard-Agglomerate Aerosols Made at High Temperatures, *Langmuir,* 20: 5933-5939.

Väisänen, O.M., A. Weber, A. Bennasar, F.A. Rainey, H.-J. Busse and M.S. Salkinoja-Salonen (1998). *J. Appl. Microbiol.* 84: 1069.

Ulrich, G.D. (1971). Theory of particle formation and growth in oxide synthesis flames, *Combustion Science and Technology,* 4: 47-57.

Umebayashi, T., T. Yamaki, H. Itoh, and K. Asai (2002). Analysis of electronic structures of 3d transition metal-doped TiO_2 based on band calculations, *J. Phys. Chem. Sol.* 63: 1909.

Virtanen, A., J. Ristimäki and J. Keskinen (2004). Method for Measuring Effective Density and Fractal Dimension of Aerosol Agglomerates, *Aerosol Science and Technology*, 38: 437-446.

Wang, S.C. and R.C. Flagan (1990). Scanning Electrical Mobility Spectrometer. *Aerosol Sci. Technol.* 13: 230-240.

Zachariah, M.R. and S. Husarewich (1991). Flame Synthesis of High Tc Superconductors. *Combustion and Flame* 87: 100-103.

Paper I

Mäkelä J. M., Keskinen H., Forsblom T. and Keskinen J.

Generation of Metal and Metal Oxide Nanoparticles by Liquid Flame Spray Process

Journal of Material Science 2004, 15: 2783-2788.

Paper II

Keskinen H., Mäkelä J. M., Vippola M., Nurminen M., Liimatainen J. K., Lepistö T., and Keskinen J.

Generation of Silver/Palladium Nanoparticles by Liquid Flame Spray

Journal of Material Research 2004, 19: 1544-1550.

Paper III

Pitkänen A, J. M. Mäkelä, M. Nurminen, A. Oksanen, K. Janka, J. Keskinen, H. Keskinen, J. K. Liimatainen, S. Hellsten and T. Määttä.

Numerical Study of Silica Particle Formation in Turbulent H_2/O_2 Flame

IFRF Combust. J., 2005, Article No 200509.

Paper IV

H. Keskinen , J.M. Mäkelä S. Hellsten, M. Aromaa, E. Levänen and T. Mäntylä

Generation of Titania Nanoparticles by Liquid Flame Spray for Photocatalytic Applications

Electrochemical Soc. Proceedings,2005-09: 491-498.

Reprinted with permission from Electrochemical Society19: 491-498.

Paper V

Keskinen H., Mäkelä J.M., Aromaa M., Ristimäki J., Kanerva T., Levänen E., Mäntylä T. and Keskinen J.

Effect of Silver Addition on the Formation and Deposition of Titania Nanoparticles Produced by Liquid Flame Spray,

In press: will be published in Journal of Nanoparticle Research 2007

Paper VI

Keskinen H., Mäkelä J.M., Aromaa M., Areva S., Teixeira C.A., Rosenholm J.B., Pore V., Ritala M., Leskelä M., Raulio M., Salkinoja-Salonen M., Levänen E., Mäntylä M., and Keskinen J.

Titania and titania-silver nanoparticle deposits made by Liquid Flame Spray and their functionality as photocatalyst for organic- and biofilm removal,

Catalysis Letters (2006) 111: 127-132.

Tampereen teknillinen yliopisto
PL 527
33101 Tampere

Tampere University of Technology
P.O. Box 527
FIN-33101 Tampere, Finland